The alternative sigma factor σ^X mediates competence shut-off at the cell pole in *Streptococcus pneumoniae*.

Calum JOHNSTON[1,2], Anne-Lise SOULET[1,2], Matthieu BERGE[1,2,3], Marc PRUDHOMME[1,2], David DE LEMOS[1,2], Patrice POLARD[1,2,4].

1. Laboratoire de Microbiologie et Génétique Moléculaires, UMR5100, Centre de Biologie Intégrative (CBI), Centre Nationale de la Recherche Scientifique (CNRS), Toulouse, France.

2. Université Paul Sabatier (Toulouse III), Toulouse, France.

3. Dept. Microbiology and Molecular Medicine, Institute of Genetics & Genomics in Geneva (iGE3), Faculty of Medicine, University of Geneva, Geneva, Switzerland.

4. Corresponding author

Keywords

Competence regulation, competence shut-off, alternative sigma factor, σ^X, DprA.

Summary

Bacterial competence for genetic transformation is a well-known species-specific differentiation program driving genome plasticity, antibiotic resistance and virulence in many pathogens. How competence regulation is spatiotemporally integrated in the cell is ill-defined. Here, we unraveled the localization dynamics of the key regulators that master the two intertwined transcription waves controlling competence in *Streptococcus pneumoniae*. The first wave relies on a stress-inducible phosphorelay system, made up of the ComD and ComE proteins, and the second is directed by an alternative sigma factor, σ^X, which includes in its regulon the DprA protein that turns off competence through interaction with phosphorylated ComE. Remarkably, we found that ComD, σ^X and DprA stably co-localize at a single cell pole over the competence period. In contrast, ComE assembles into dynamic patches in the cell periphery, colocalizing temporarily with DprA and ComD at the pole. Furthermore, we provide evidence that σ^X directly conveys DprA polar anchoring. Through this protein targeting function, σ^X is shown to be actively involved in the timely shut-off of the competence cycle, hence preserving cell fitness. Altogether, this study unveils an unprecedented role for a bacterial transcription σ factor in spatially coordinating the negative feedback loop of its own genetic circuit.

Introduction

In bacteria, sigma (σ) factors are essential transcription effectors that direct the RNA polymerase to and activate RNA synthesis at specific genes promoters. All bacterial species encode a single, highly conserved σ factor that drives the expression of house-keeping genes essential for vegetative growth and cell homeostasis. In addition, many bacteria encode a variable set of alternative σ factors that control specific regulons, providing appropriate properties to the cells in response to various stimuli. These alternative σ factors play pivotal roles in the multifaceted lifestyles of bacteria. They trigger specific developmental programs, such as sporulation or biofilm formation, as well as adapted responses to multiple types of stress and virulence in some pathogenic species (Kazmierczak et al., 2005). How these alternative σ factors are activated in the cell has been extensively studied, revealing multiple mechanisms underlying their finely tuned regulation(Österberg et al., 2011a). However, how these mechanisms are orchestrated spatiotemporally within the cell remains poorly understood.

The human pathogen *Streptococcus pneumoniae* (the pneumococcus) possesses a unique alternative σ factor σ^X (Lee and Morrison, 1999). It is key to the regulatory circuit controlling the transient differentiation state of competence. Pneumococcal competence is induced in response to multiple types of stresses, such as antibiotic exposure (Prudhomme et al., 2006; Slager et al., 2014). This induction modifies the transcriptional expression of up to 17% of genes (Aprianto et al., 2018a; Dagkessamanskaia et al., 2004a; Peterson et al., 2004; Slager et al., 2019). Competence is a key feature in the lifestyle of pneumococci as it promotes natural transformation, a horizontal gene transfer process widespread in bacteria that facilitates adaptation by acquisition of new genetic traits (Johnston et al., 2014). In addition, pneumococcal competence development provides the cells with the ability to attack non-competent cells, a scavenging property defined as fratricide (Claverys and Håvarstein, 2007), is involved in biofilm formation (Aggarwal et al., 2018; Vidal et al., 2013) and virulence (Johnston et al., 2018; Lin et al., 2016; Lin and Lau, 2019; Zhu et al., 2015).

Pneumococcal competence induction is primarily regulated by a positive feedback loop involving the genes encoded by the *comAB* and *comCDE* operons (Figure 1A). The *comC* gene codes for a peptide pheromone coordinating competence development within the growing cell population. This peptide, accordingly named CSP (Competence Stimulating Peptide), is secreted by the dedicated ComAB transporter (Hui et al., 1995). After export, it promotes autophosphorylation of the membrane-bound two-component system (TCS) histidine kinase (HK) ComD, which in turn phosphorylates its cognate intracellular response regulator (RR) ComE (Figure 1A). Phosphorylated ComE (ComE~P) specifically induces the expression of 25 genes, which include the *comAB* and *comCDE* operons, generating a positive feedback loop that controls competence development. Conversely, unphosphorylated ComE acts as repressor of its own regulon, the expression of which is thus modulated by the ComE/ComE~P ratio (Martin et al., 2013). The ComE regulon includes two identical genes encoding σ^X, named *comX1* and *comX2* (Lee and Morrison, 1999). The σ^X regulon comprises ~60 genes, with ~20 involved in natural transformation (Claverys et al., 2006; Peterson et al., 2004), 5 in fratricide (Claverys and Håvarstein, 2007) but the majority having undefined roles. The reason why the σ^X-encoding gene is duplicated is unknown, the inactivation of one of them having no impact on transformation (Lee and Morrison, 1999). To fully activate transcription, σ^X needs to be assisted by ComW, another protein whose production is controlled by ComE~P (Luo et al., 2004). ComW is proposed to help σ^X association with the RNA polymerase at promoter sequences presenting the consensual 8 bp *cin* box motif (Peterson et al., 2004; Sung and Morrison, 2005). Altogether, ComE~P and σ^X trigger two successive waves of competence (*com*) gene transcription, commonly referred to as early and late, respectively. Importantly, competence shut-off is mediated by the late *com* protein DprA (Mirouze et al., 2013; Weng et al., 2013), which directly interacts with ComE~P to turn-off ComE~P-dependent transcription (Mirouze et al., 2013). In addition to defining the negative feedback loop of the pneumococcal competence regulatory circuit, DprA also plays a crucial, conserved role in transformation by mediating RecA polymerization onto transforming ssDNA to facilitate homologous recombination (Mortier-Barrière et al., 2007; Cheruel et al., 2012) (Figure 1A). Over 8,000 molecules

of DprA are produced per competent cell (Mirouze et al., 2013). Although only ~300-600 molecules were required for optimal transformation, full expression of *dprA* was required for optimal competence shut-off (Johnston et al., 2018). Uncontrolled competence induction in cells lacking DprA results in a large *in vitro* growth defect, and high cellular levels of DprA thus maintain the fitness of the competent population and of resulting transformants (Johnston et al., 2018). In addition, inactivation of *dprA* was shown to be highly detrimental for development of pneumococcal infection, dependent on the ability of cells to develop competence (Lin and Lau, 2019; Zhu et al., 2015). Together, these studies showed that the DprA-mediated shut-off of pneumococcal competence is key for pneumococcal cell fitness.

A hallmark of pneumococcal competence is its tight temporal window, which lasts less than 30 minutes in actively dividing cells (Alloing et al., 1998; Håvarstein et al., 1995). How this regulation is coordinated within the cell remains unknown. Here, we studied the choreography of pneumococcal competence induction and shut-off at the single cell level by tracking the spatiotemporal localization of the main effectors of these processes, DprA, σ^X, ComW, ComD, ComE and exogenous CSP. Remarkably, DprA, σ^X, ComD, CSP and to some extent ComE were found to colocalize at a single cell pole during competence. This study revealed that the entire pneumococcal competence cycle occurs at cell pole, from its induction triggered by ComD, ComE and CSP to its shut-off mediated by DprA and assisted by σ^X. In this regulatory mechanism, σ^X is found to exert an unprecedented role for a σ factor. In addition to directing the transcription of the *dpr*A gene, σ^X associates with and anchors DprA at the same cellular pole where ComD and CSP are located, allowing this repressor to interact with newly activated ComE~P and promoting timely extinction of the whole transcriptional regulatory circuit of competence.

Results

DprA displays a polar localization in competent cells, which correlates with competence shut-off.

To investigate the localization of DprA during competence in live cells, we used a fluorescent fusion protein DprA-GFP, produced from the native *dprA* locus (Figure S1A). DprA-GFP was synthesized during competence and remained stable up to 90 minutes after induction (Figure 1B), similarly to wildtype DprA (Mirouze et al., 2013), without degradation (Figure S1B). A strain possessing DprA-GFP was almost fully functional in transformation (Figure S1C), but partially altered in competence shut-off (Figure S1D). In pneumococcal cells induced with exogenous CSP, the peak of competence induction occurs 15-20 minutes after induction. 15 minutes after competence induction, DprA-GFP showed a diffuse cytoplasmic localization, punctuated by discrete foci of varying intensity (Figure 1C). The distribution and localization of DprA-GFP foci was analyzed by MicrobeJ (Ducret et al., 2016), with results presented as focus density maps ordered by cell length. Spots represent the localization of a DprA-GFP focus on a representative half pneumococcal cell, while spot colour represents density of foci at a particular cellular location. DprA-GFP foci were present in 70% of cells, predominantly at a single cell pole (Figure 1DE). To ascertain whether the polar localization of DprA-GFP was due to the GFP tag or represented functional localization, we carried out immunofluorescence microscopy with competent cells possessing wildtype DprA using α–DprA antibodies. Results showed that native DprA exhibited a similar accumulation pattern as the DprA-GFP foci upon competence induction (Figure 1F).

Next, to explore the relation between these foci and the dual role of DprA in transformation and competence regulation, we investigated focus formation in cells possessing a previously published mutation in DprA impairing its dimerization ($DprA^{AR}$) (Quevillon-Cheruel et al., 2012). This mutant strongly affected both transformation and competence shut-off (Mirouze et al., 2013; Quevillon-Cheruel et al., 2012). Results showed that 15 minutes after competence induction, $DprA^{AR}$-GFP did not form foci, despite being produced at wildtype levels (Figure S1E). DprA thus accumulates at the cell pole during competence, dependent on its ability to dimerize. To explore whether the polar foci of

147 DprA were involved in its role in transformation, or competence shut-off, we began by investigating
148 how a *dprA*^{QNQ} mutation, specifically abrogating the interaction between DprA and RecA and thus
149 affecting transformation (Quevillon-Cheruel et al., 2012), affected the localization of DprA-GFP. 15
150 minutes after competence induction, the DprA^{QNQ}-GFP mutant formed polar foci at wildtype levels
151 (Figure S1F). In addition, the inactivation of *comEC*, encoding for an essential protein of the
152 transmembrane DNA entry pore (Pestova and Morrison, 1998), or *recA*, encoding the recombinase
153 with which DprA interacts during transformation (Mortier-Barrière et al., 2007), did not alter the
154 frequency or localization of DprA-GFP foci (Figure S1GH). Altogether, these results suggested that the
155 polar foci of DprA-GFP were not related to the DNA entry or recombination steps of transformation
156 but could be linked to competence shut-off.

157 We recently reported that optimal competence shut-off relies on the maximal cellular
158 concentration of DprA (~8000 molecules), but this level could be reduced by 10 fold while still
159 maintaining wildtype frequency of transformation (Johnston et al., 2018). This conclusion was
160 obtained by expressing *dprA* under the control of the IPTG-inducible P_{lac} promoter (*CEP*$_{lac}$-*dprA*), which
161 enables the modulation of the cellular concentration of DprA by varying IPTG concentration in the
162 growth medium. Here, we reproduced these experiments with the DprA-GFP fusion, to test whether
163 its concentration correlates with the formation of polar foci in competent cells. The expression,
164 transformation and competence profiles of a *dprA*$^{-}$ mutant strain harbouring the ectopic *CEP*$_{lac}$-*dprA*-
165 *gfp* construct in varying concentrations of IPTG (Figure S2ABC) were equivalent to those reported
166 previously for *CEP*$_{lac}$-*dprA* (Johnston et al., 2018). Notably, a steady decrease in DprA-GFP foci was
167 observed as IPTG was reduced (Figure 2AB). When comparing the cellular localization of DprA-GFP foci,
168 a sharp reduction in the proportion of polar foci was observed as IPTG was reduced, with most of the
169 remaining foci observed at midcell and appearing weaker in intensity (Figure 2AC). This shift correlated
170 with a progressive loss of competence shut-off (Figure S2C), presenting a strong link between the
171 presence of polar DprA-GFP foci and the shut-off of pneumococcal competence. Altogether, these

172 results strongly support the notion that the polar foci of DprA-GFP represent the subcellular site where
173 DprA mediates competence shut-off.

174 Finally, to further explore the temporal dynamics of these DprA-GFP foci, their distribution
175 within competent cells was analyzed over the competence period and beyond. The results are
176 presented in Figure 3A as focus density maps ordered by cell length. The number of cells with foci, as
177 well as their intensity, was found to increase gradually to reach a maximum of 74% at 30 minutes after
178 competence induction (Figure 3A), with the majority of cells possessing a single focus that persisted
179 long after induction (Figure 3B). Notably, the DprA-GFP foci localization pattern rapidly evolved from
180 a central position to a single cell pole (Figure 3C). DprA-GFP foci were not observed in a particular cell
181 type, with found in small, large or constricted cells throughout competence (Figure 3C). Finally,
182 tracking DprA-GFP foci formed in the cells after 10 minutes of competence induction by time-lapse
183 microscopy showed that once generated, they remained static over 20 minutes (Figure S1IJ, Movie 1).
184 In conclusion, DprA-GFP forms discrete and static polar foci during competence, with most cells
185 possessing a single focus. This polar localization of DprA correlates with its regulatory role in
186 competent shut-off.

187

188 ***The polar localization of DprA-GFP requires induction of the late* com *genes***

189 Transcriptional expression of *dprA* is only detected during competence (Aprianto et al., 2018a;
190 Dagkessamanskaia et al., 2004a; Peterson et al., 2004). To explore whether a competence-specific
191 factor was required for the formation of polar DprA-GFP foci during competence, *dprA-gfp* was
192 ectopically expressed from a promoter inducible by the BIP peptide in *dprA*$^{-}$ cells. This BIP-derived
193 induction mimics rapid, strong induction by CSP during competence (Johnston et al., 2016). These cells
194 were found to produce stable DprA-GFP after exposure to BIP, and upon addition of CSP to the growth
195 medium, to transform at wild-type levels and to partially shut-off competence (Figure S3). However,
196 BIP-induced production of DprA-GFP in the absence of CSP resulted in the formation of weak, barely

197 detectable polar foci in only 10% of non-competent cells (Figure 4AB). In comparison, 47% of cells
198 producing DprA-GFP during competence formed bright polar foci (Figure 4AB). This stark increase in
199 DprA-GFP foci showed that a competence-specific factor was crucial for their formation and anchoring
200 at the cell pole. To explore whether the competence-specific factor needed for the polar localization
201 of DprA-GFP in competent cells was part of the early or late *com* regulons, we generated two
202 constructs allowing us to artificially control DprA-GFP expression and either one or the other of these
203 two connected regulons (Figure 4CD and Supplementary methods). Observation of DprA-GFP in
204 conditions where only late *com* genes were induced revealed the presence of polar foci at wildtype
205 levels (Figure 4EF). Conversely, no foci were observed when DprA-GFP was ectopically expressed with
206 only the early *com* genes (Figure 4E), showing that late *com* regulon expression was required for the
207 polar accumulation of DprA-GFP.

208

209 ***The polar localization of DprA-GFP depends on the alternative sigma factor σ^X***

210 The late *com* regulon is comprised of 62 genes, organized in 18 operons (Claverys et al., 2006;
211 Dagkessamanskaia et al., 2004b; Peterson et al., 2004). To identify the hypothetical late *com* gene
212 product needed for DprA localization at the cell pole, the *cin* boxes that define the late *com* promoters
213 were individually mutated, generating a panel of 18 mutant strains, each lacking the ability to induce
214 a specific late *com* operon. The inactivation was validated by comparing transformation efficiency in
215 three strains, where *cin* box inactivation mirrored gene knockout levels (Table S1, and Supplementary
216 methods). Visualization of the red fluorescent fusion DprA-mKate2 showed that in all 18 mutants,
217 DprA-mKate2 formed foci at levels and localization comparable to wildtype (Table S2). This result
218 contrasted with our previous result (Figure 4E), which suggested that expression of the late *com*
219 regulon was required for formation of polar DprA-GFP foci, causing us to revisit our interpretation of
220 Figure 4C-F. In fact, to express only the early *com* regulon, we inactivated *comX1*, *comX2* and *comW*
221 (Figure 4C), so this strain produced only early *com* proteins, except σ^X and ComW, and lacked DprA-

GFP foci (Figure 4E). Conversely, to express only the late *com* regulon, we ectopically expressed *comX* and *comW* (Figure 4D), so this strain produced the late *com* regulon but also the early *com* proteins σ^X and ComW and displayed polar DprA-GFP foci at wildtype levels (Figure 4EF). This led us to consider that the only proteins whose presence correlated directly with the presence of polar DprA-GFP foci were thus σ^X and ComW.

To first investigate whether ComW played a role in the formation of polar DprA-GFP foci, the *comW* gene was inactivated in a strain possessing a *rpoD*^{A171V} mutation, enabling σ^X-RNA polymerase interaction and resulting in late *com* regulon expression in the absence of ComW (Tovpeko et al., 2016). DprA-GFP expressed from the native locus still formed polar foci in this strain at levels comparable to the wildtype strain (Figure S4A). ComW was thus not required for the formation of DprA-GFP foci. In light of this, the only remaining candidate whose presence in competent cells correlated directly with formation of polar DprA-GFP foci was σ^X. Thus, to determine if σ^X alone was necessary and sufficient to localize DprA-GFP to the cell poles, both *comX* and *dprA-gfp* or *dprA-gfp* alone were expressed in non-competent *rpoD*^{wt} cells. Western blot analysis using α-SsbB antibodies indicated that the late *com* regulon was weakly induced when σ^X was ectopically produced in the absence of *comW* (Figure S4B). Cells producing DprA-GFP alone showed polar DprA-GFP foci in 10% of cells (Figure 5A). In contrast, DprA-GFP foci were formed in 37% of cells when σ^X was also produced in non-competent cells (Figure 5A). Importantly, induction of competence in both of these strains resulted in similar foci numbers (Figure S4D). Altogether, this result suggested that σ^X alone was sufficient to stimulate polar foci of DprA-GFP, highlighting an unexpected role for this early competence σ factor only known to act in concert with ComW to induce late competence gene transcription.

σ^X mediates the localization of DprA at the cell pole of competent cells

To investigate how σ^X could be involved in the polar localization of DprA-GFP, we explored how it localized in competent cells. To this end, we generated a *comX1-gfp* construct at the native *comX1*

247 locus combined with a wildtype *comX2* gene (Figure S5 and Supplementary results). Remarkably, σ^X-
248 GFP formed bright polar foci 15 minutes after competence induction (Figure 5A), reminiscent of those
249 formed by DprA-GFP (Figure 1C). A time-course experiment after competence induction showed that
250 σ^X-GFP localized to the cell pole as soon as 4 minutes after CSP addition (Figure 5B), when DprA-GFP
251 forms weak foci at midcell (Figure 3A). In contrast, a ComW-GFP fusion protein displayed a diffuse
252 cytoplasmic localization in the majority of competent cells, with only 7% of cells possessing weak foci
253 at the cell poles (Figure S5A and Supplementary results). Thus, σ^X-GFP localizes to the cell pole without
254 its partner in transcriptional activation ComW, despite the fact that σ^X is an alternative sigma factor
255 directing RNA polymerase to specific promoters on the chromosome.

256 Analysis of σ^X-GFP foci distribution showed that they are detected in up to 51% of cells 10
257 minutes after competence induction, with most cells possessing a single focus (Figure 5BC). The
258 number of cells with foci decreased steadily after this point (Figure 5BCD), contrasting with polar DprA-
259 GFP which remained stable over 60 minutes after induction. Importantly, σ^X-GFP continued to form
260 polar foci in a strain lacking *dprA* (Figure 5E), showing that σ^X does not depend on DprA for its
261 localization. Together, these results strongly supported the notion that σ^X promotes the targeting and
262 assembly of DprA-GFP foci at the cell pole. To further explore this hypothesis, we co-expressed DprA-
263 mTurquoise and σ^X-YFP fluorescent fusions in the same cells and found that 86% of DprA-mTurquoise
264 foci colocalized with σ^X-YFP foci (Figure 5F). DprA and σ^X are thus present at the same pole of the cell
265 at the same time and the polar accumulation of DprA molecules in competent cells depends on σ^X.
266 These results suggested that σ^X could interact with DprA to anchor it to the pole of competent cells.
267 The potential interaction between σ^X and DprA was tested in live competent pneumococcal cells in
268 pull-down experiments. To achieve this, we used GFP-TRAP magnetic beads (Chromotek) to purify σ^X-
269 GFP from competent cells expressing either wildtype DprA or, as a control, the $DprA^{AR}$ mutant that did
270 not accumulate at the cell pole (Figure S1). Results showed that wildtype DprA co-purified with σ^X-GFP
271 from competent cells extracts, but $DprA^{AR}$ did not, revealing that σ^X and DprA interact in live competent

pneumococci (Figure 5H). Taken together, these findings reveal that σ^X is responsible for the accumulation of DprA at the cell pole during competence.

Pneumococcal competence induction occurs at the cell pole

We have shown that DprA localization at a single cell pole correlates with the shut-off of competence (Figure 2). Since DprA interacts directly with ComE~P to mediate competence shut-off (Mirouze et al., 2013), this raised the question of the subcellular localization of ComD and ComE, which define a TCS controlling competence regulation. To first explore the localization of ComE in competent cells, a strain was generated expressing a functional *comE-gfp* fluorescent fusion at the native *comE* locus (Figure S6 and Supplementary results). In competent cells, ComE-GFP formed patches around the periphery of the cell, often at the cell pole (Figure 6AB and S7A). A time-lapse experiment showed that these patches were dynamic, navigating around the cell membrane over time (Movie 2). Next, to explore the sub-cellular localization of ComD, we generated a strain expressing *gfp-comD* at the native *comD* locus (Figure S6AC and Supplementary results). The resulting GFP-ComD fusion displayed partial functionality in competence induction and transformation (Figure S6DE). In contrast to ComE-GFP, GFP-ComD formed distinct polar foci of varying intensity in 57% of cells (Figure 6AB), a localization pattern reminiscent of those observed with DprA-GFP and σ^X-GFP (Figures 1 and 5, respectively). Since GFP-ComD was not fully functional, we also analyzed the localization of a synthetic fluorescent exogenous CSP peptide (CSP-HF, Figure S6F) in parallel, to track its interaction with ComD at the cell surface. This fluorescent peptide was found to accumulate at a single cell pole in the majority of competent, wildtype cells (Figure 6AB). In addition, this accumulation was dependent on the presence of ComD (Figure 6A), showing that the polar accumulation of the partially functional GFP-ComD fusion represented a functional subcellular localization during competence. In addition, most cells with ComD-GFP foci possessed a single focus (Figure 6C), which persisted after the shut-off of competence (Figure S7B). Altogether, these findings revealed that activation of the positive feedback loop of

297 competence triggered by CSP interaction with ComD to phosphorylate ComE occurs at the cell pole.
298 Since a single pole is mainly targeted by ComD, this also raised the question of its co-localization with
299 ComX and DprA.

300

301 ***DprA colocalizes with ComD and CSP during competence***

302 To explore the hypothesis that DprA accumulates at the same pole as ComD to mediate
303 competence shut-off, we performed colocalization analyses of DprA with ComE, ComD or CSP
304 respectively, in the same competent cells. Although ComE-YFP foci were dynamic and their localization
305 difficult to analyze, 20% of DprA-mTurquoise foci were nonetheless found to colocalize with ComE-YFP
306 at the cell pole, showing that these proteins can be found at the same pole in the same cells (Figure
307 6D). In contrast, 76% of DprA-mTurquoise foci colocalized with YFP-ComD (Figure 6E), showing that
308 these foci form at the same pole in the majority of cells. In addition, 73% of DprA-GFP foci colocalized
309 with CSP-HF (Figure 6F). Taken together, these results showed that DprA colocalizes strongly with
310 ComD, generally at one cell pole during pneumococcal competence, further suggesting that the
311 localization of DprA to this cellular location, mediated by σ^X, facilitates pneumococcal competence
312 shut-off. The localization of DprA at the cell pole where ComD appears to interact with CSP means that
313 DprA is present at the time and place that neophosphorylated ComE~P is produced, allowing DprA to
314 interact with the activated regulator at the cell pole and prevent it from accessing its genomic targets,
315 facilitating shut-off.

316

317 ***Two copies of* comX *are required for optimal competence shut-off***

318 A distinct hallmark of the single pneumococcal alternative sigma factor σ^X of *S. pneumoniae* is
319 that it is produced from two distinct and strictly identical genes, at two distinct loci in the
320 pneumococcal genome, known as *comX1* and *comX2* (Lee and Morrison, 1999). However, inactivation

of either of these genes had no effect on the efficiency of transformation as previously reported (Lee and Morrison, 1999) (Figure 7A), suggesting that the expression of either *comX1* or *comX2* is sufficient to induce the late *com* regulon to a level ensuring optimal transformation. Having established that σ^X plays a second key role in competence shut-off, we explored whether this role required both *comX* genes. Inactivation of either *comX* gene not only slightly reduced the peak of late *com* gene expression but also markedly delayed the rate of competence shut-off (Figure 7B), revealing that reducing the cellular level of σ^X impacts competence shut-off efficiency, presumably because less σ^X is present to promote accumulation of DprA at the cell poles. In addition, this unregulated competence shut-off of single *com*X mutants is accompanied by a reduced growth rate of the cell population, consistent with an alteration of cell fitness linked to altered competence shut-off (Johnston et al., 2018). In conclusion, this finding suggests that pneumococci possess two copies of *comX* to optimize DprA-mediated competence shut-off and maintain the fitness of competent cells.

Pre-competence expression of DprA and σ^X antagonizes competence induction

This study has uncovered a new functional role of pneumococcal σ^X in facilitating DprA-mediated inactivation of ComE-P at the cell pole. To obtain further proof that polar DprA plays a role in competence shut-off, we reasoned that if σ^X localizes DprA to the cell pole to allow it to interact with neophosphorylated ComE~P, then early ectopic expression of DprA and σ^X should antagonize competence induction by interfering with early *com* regulon induction. To test this hypothesis, we expressed DprA alone or both DprA and σ^X prior to CSP addition to the growth medium (Figure 7C), referred hereafter as a pre-competence expression. Pre-competence production of DprA alone did not affect competence induction as shown by monitoring luciferase controlled by an early *com* promoter (Figure 7D). In these conditions, minimal amounts of DprA accumulated at the cell pole (Figure 5A). However, pre-competence expression of both DprA and σ^X resulted in a significantly slower induction of competence (Figure 7E). This suggested that σ^X-mediated pre-localization of DprA to the cell poles

in pre-competent cells, as shown in Figure 4G, markedly antagonized CSP induction of competence by allowing DprA to interact with and inactivate neophosphorylated ComE~P. Inactivation of *comW* in this strain to minimize late *com* gene expression did not alter the profiles (Figure 7F), showing that the observed effect was directly attributable to the role of σ^X in localizing DprA to the cell poles. Altogether, these findings further prove that in live cells the targeting of pneumococcal DprA to the cell pole, promoted by σ^X anchored at this cellular location, mediates the timely antagonization of the competence induction signal.

Discussion

The cell pole defines a competence regulation hub in S. pneumoniae

We report here a spatiotemporal analysis of competence regulation in live pneumococcal cells. We found that the positive regulators ComD, ComE and σ^X, which control the early and late competence expression waves, and the negative regulator DprA colocalize during competence at one cell pole to temporally coordinate its development and shut-off. We have shown that the initial stages of competence induction, relying on the CSP-induced phosphorelay between ComD and ComE, occur at the cell pole (Figure 7G). Most importantly, this study uncovered an unexpected second role for σ^X in competence regulation. In addition to controlling the transcription of the late *com* gene *dprA*, σ^X also mediates the accumulation of DprA molecules mostly at the same pole as ComD, a mechanism that facilitates competence shut-off. σ^X thus controls both induction of the late *com* regulon and the shut-off of the early *com* regulon, including thereby its own expression and by consequence that of its regulon. We found that the σ^X-directed polar localization of DprA in the vicinity of ComD correlates with its role in competence shut-off. We propose that this targeting favours DprA interaction between DprA and neosynthesized ComE~P to promote efficient shut-off (Figure 7H). Importantly, we previously reported that DprA-mediated competence shut-off is crucial to the fitness of competent cells (Johnston et al., 2018; Mirouze et al., 2013), and we revealed here that this vital role of DprA in

actively limiting the competence window is orchestrated at the cell pole, which defines a coordination hub of competence regulation. Unexpectedly, DprA is targeted to this hub by σ^X, describing an unprecedented role for an alternative sigma factor.

The pneumococcal polar competence regulation hub is focused around the histidine kinase ComD

An important finding is the discrete accumulation of the pneumococcal HK ComD at the cell pole during competence (Figure 6AB). The localization of HKs has not been extensively studied, but few HKs of two-component signaling systems (TCS) have been found to accumulate at the cell pole. One well-documented example is the *Escherichia coli* HK CheA, which is involved in chemotaxis. CheA localizes along with its cognate RR CheY to a single cell pole, forming a chemotactic cluster with a variety of chemoreceptors. CheY stimulates the production of flagellae at the opposite cell pole, driving chemotaxis (Baker et al., 2006). Another example is the HK PilS in *Pseudomonas aeruginosa*, which also accumulates at the cell pole, and along with its cognate cytoplasmic RR PilR, regulates expression of polar pili (Boyd, 2000). Although ComD tethering at one cell pole is similar to CheA and PilS, major differences exist between these three TCS system. Firstly, regarding how their RRs localize, ComE presents a different localization pattern than CheY and PilR, assembling into patches close to the inner side of the cell membrane and focusing dynamically on the cell pole (Figure 6A and Movie 2). ComE phosphorylation by ComD promotes its dimerization and switch into a transcriptional activator (Martin et al., 2013). ComE~P dimers should then leave the cell pole to interact with genomic targets and turn on early *com* gene expression, producing σ^X and ComW, which then cooperate to turn on late *com* gene expression. Secondly, the ComDE TCS induces its own expression, generating a positive feedback loop (Claverys et al., 2006; Martin et al., 2013), and leading to the strong, rapid induction of competence (Dagkessamanskaia et al., 2004b; Peterson et al., 2004). As found here, this leads to the accumulation of the regulatory proteins at the cell pole hub. In addition, the ComDE TCS controls a complex, multi-faceted genetic program involving the altered expression of 17% of the genome (Aprianto et al., 2018b)

and is present at a unique cell pole, while the actors of transformation are present at midcell (Bergé et al., 2013). Finally, it is possible that the polar localization of the competence regulatory hub is dictated by the very nature of the competence regulation mechanism itself. This localization could be linked to the transient nature of pneumococcal competence. A spatiotemporally controlled localization for this process would provide a mechanism to allow initial induction followed by repression, thus preventing toxicity. It is also possible that the purpose of polar accumulation of σ^X is to limit the circulating levels of σ^X. Polar accumulation of σ^X may thus protect the cell from a potentially dangerous hyper-competent state at two levels, firstly by promoting polar DprA accumulation to facilitate shut-off, and secondly by sequestering σ^X itself to prevent over-induction of the late *com* regulon. Although the factor localizing σ^X to the cell pole is unknown, it could be considered an anti-sigma factor in this light. Anti-sigma factors can control alternative sigma factors by interacting directly with them to sequester them to prevent activity until a specific signal is received (Österberg et al., 2011b). Although ComD goes to the same pole as σ^X, it is not the anchor directing σ^X to the pole, since DprA (and thus σ^X) still localizes to the cell pole in the absence of early *com* genes (Figure 4EF).

Two copies of comX *ensure optimal fitness of competent cells*

This study has uncovered a second role for σ^X in the shut-off of pneumococcal competence, besides its transcriptional role with ComW, which is to associate with the RNA polymerase and direct the expression of the late *com* regulon. This second role is independent of ComW. It promotes accumulation of DprA at the cell pole to facilitate competence shut-off. Pneumococci possess two identical copies of *comX* at distinct locations within the genome, called *comX1* and *comX2* (Lee and Morrison, 1999). It has remained unclear why two copies exist, since inactivation of a single copy of *comX* does not affect transformation efficiency (Figure 7A) (Lee and Morrison, 1999). The finding of a second role for σ^X in the shut-off of competence suggests a different reason for this duplication, since both copies of *comX* are required for optimal competence shut-off (Figure 7B). We thus propose that

two copies of *comX* are maintained within the genome to optimize the shut-off of competence. Since unregulated competence is toxic for the cell (Johnston et al., 2018), two copies of *comX* provide a fail-safe in case of loss or inactivation of one *comX* gene by transformation or spontaneous mutation, allowing the cell to nonetheless exit the competent state. In light of the second role of σ^X uncovered here, two copies of *comX* provide a simple yet elegant means for *S. pneumoniae* and close relatives to ensure they are always equipped to survive competence, allowing cells to reap the potential benefits of competence without the fitness cost associated with unregulated competence.

Polar accumulation of DprA and ComD and heterogneity in a post-competence cell population

The σ^X-mediated accumulation of DprA in foci at the cell pole depends on a high concentration of DprA molecules in the cell, resulting from the σ^X-driven transcription of the *dprA* gene (Figure 2). This dual feature implies that polar DprA foci are not formed immediately during competence, in line with our findings (Figure 3). We suggest that this short delay provides the opportunity for ComD to phosphorylate ComE and induce competence, before DprA arrives at the cell pole to facilitate shut-off. In addition, the foci formation is dependent on the ability of DprA to dimerize, which alters its both its role in transformation via interaction with RecA and its role in competence shut-off via interaction with ComE (Mirouze et al., 2013; Quevillon-Cheruel et al., 2012). However, DprA polar foci formation is independent of the presence of the transformation pore protein ComEC or the recombinase RecA, suggesting that the observed foci are not linked to the conserved role of DprA in transformation (Figure S1). In addition, the loss of polar foci when reducing cellular levels of DprA-GFP correlates with the loss of competence shut-off, strongly supporting the proposal that DprA accumulation at the cell pole underpins its negative feedback role in competence regulation (Figure 2 and S2).

In a competent population, the presence and intensity of DprA-GFP foci varies from cell to cell (Figure 3). The same heterogeneity is observed with GFP-ComD foci (Fig. S7). Indeed, at the peak of CSP-induced competence, a quarter of cells do not present detectable DprA-GFP or GFP-ComD foci

and, in the other cells, the foci exhibit different level of brightness (Figures 3 and S7). In addition, foci are observed in all cell types, meaning that their formation is not determined by a particular stage of the cell-cycle. This highlights a heterogeneity in the pneumococcal competent cell population. Furthermore, DprA-GFP and GFP-ComD foci persist in many cells at least 30 minutes after the shut-off of competence (Figure 3 and S7). It has been shown previously that post-competent cells are unable to respond to CSP for a period of time after they shut-off competence, a phenomenon known as 'blind to CSP' (Chen and Morrison, 1987; Fox and Hotchkiss, 1957). We suggest that the heterogeneity of polar DprA and ComD accumulation could play a role in this phenomenon. Polar DprA accumulation in a majority of cells could prevent cells from responding to CSP by immediately antagonizing neosynthesized ComE~P, while cells lacking ComD foci may not respond optimally to the competence signal. Our findings explain the suggestion made previously based on a mathematical model simulating competence regulation that a high amount of DprA played a role in this phenomenon (Weyder et al., 2018). This notion is supported by the fact that co-expression of DprA and σ^X prior to CSP addition to the cell culture antagonized competence development (Figure 7C-F). Furthermore, since not all post-competent cells possess detectable polar foci of DprA-GFP or GFP-ComD, we suggest that whether sufficient DprA or ComD has accumulated at the pole of a particular cell should govern whether this cell can respond to an external CSP signal and is thus receptive to a second wave of competence. This produces a mixture of competent and non-competent cells, which may maximize the potential survival of a pneumococcal population.

Concluding remarks

In this study, we have shown that the entire pneumococcal competence regulatory cycle occurs at a single cell pole. This generates an asymmetry at the poles of a competent cell, which can be transmitted to future generations and impact the ability to respond to subsequent competence signals. In addition, we have uncovered a key second role for the competence-dedicated alternative

sigma factor σ^X that actively localizes DprA to the polar competence regulatory hub to facilitate competence shut-off. This regulatory mechanism, involving two proteins with other conserved roles in competence and transformation respectively, is pivotal to optimal competence shut-off and maintains the fitness of competent cells. This finding represents the first example of an alternative sigma factor playing a central role in the extinction of the signal on which its own production depends and broadens our knowledge of the regulatory roles played by bacterial alternative sigma factors.

Materials and Methods

Bacterial strains, transformation and competence

The pneumococcal strains, primers and plasmids used in this study can be found in Table S3. Standard procedures for transformation and growth media were used (Martin et al., 2000). In this study, cells were rendered unable to spontaneously develop competence either by deletion of the *comC* gene (*comC0*) (Dagkessamanskaia et al., 2004a) or by replacing the *comC* gene which encodes CSP1 with an allelic variant encoding CSP2 (Pozzi et al., 1996), since ComD1 is unable to respond to CSP2 (Johnsborg et al., 2006; Weyder et al., 2018). Both of these alterations render cells unable to produce CSP. Unless described, pre-competent cultures were prepared by growing cells to an OD_{550} of 0.1 in C+Y medium (pH 7) before 10-fold concentration and storage at –80°C as 100 µL aliquots. Antibiotic concentrations (µg mL^{-1}) used for the selection of *S. pneumoniae* transformants were: chloramphenicol (Cm), 4.5; erythromycin, 0.05; kanamycin (Kan), 250; spectinomycin (Spc), 100; streptomycin (Sm), 200; trimethoprim (Trim), 20. For the monitoring of growth and *luc* expression, precultures were gently thawed and aliquots were inoculated (1 in 100) in luciferin-containing (Prudhomme and Claverys, 2007) C+Y medium and distributed (300 ml per well) into a 96-well white microplate with clear bottom. Transformation was carried out as previously described (Martin et al., 2000). 100 µL aliquots of pre-competent cells were resuspended in 900 µL fresh C+Y medium with 100 ng mL^{-1} CSP and appropriate IPTG concentrations and incubated at 37°C for 10 min. Transforming DNA

was then added to a 100 µL aliquot of this culture, followed by incubation at 30°C for 20 min. Cells were then diluted and plated on 10 mL CAT agar with 5% horse blood and appropriate concentrations of IPTG before incubation at 37°C for 2 h. A second 10 mL layer of CAT agar with appropriate antibiotic was added to plates to select transformants, and plates without antibiotic were used as comparison to calculate transformation efficiency where appropriate. Plates were incubated overnight at 37°C. To compare transformation efficiencies, transforming DNA was either R304 (Mortier-Barrière et al., 1998, p.) genomic DNA or a 3,434 bp PCR fragment amplified with primer pair MB117-MB120 as noted (Marie et al., 2017), both possessing an *rpsL41* point mutation conferring streptomycin resistance. To track competence profiles, a previously described protocol was used (Prudhomme and Claverys, 2007). Relative luminescence unit (RLU) and OD values were recorded throughout incubation at 37°C in a Varioskan luminometer (ThermoFisher). The *comC-luc* and *ssbB-luc* reporter genes were transferred from R825 or R895 as previously described (Bergé et al., 2002; Chastanet et al., 2001). *CEP$_{lac}$-dprA-gfp* strains were grown in varying concentrations of IPTG from the beginning of growth, as previously described (Johnston et al., 2018). Detailed information regarding the construction of new plasmids and strains can be found in the Supplementary Information.

Fluorescence microscopy and image analysis

Pneumococcal precultures grown in C+Y medium at 37°C to an OD_{550} of 0.1 were induced with either CSP (100 ng mL^{-1}) or BIP (250 ng mL^{-1}) peptide. At indicated times post induction, 1 mL samples were collected, cooled down by addition of 500 mL cold medium, pelleted (3 min, 3,000 g) and resuspended in 1 mL C+Y medium. 2 µL of this suspension were spotted on a microscope slide containing a slab of 1.2% C+Y agarose as previously described (Bergé et al., 2013) before imaging. Unless stated, images were visualized 15 minutes after competence induction, at the peak of competence gene expression. To generate movies, images were taken of the same fields of vision at varying time points during incubation at 37°C. Images were captured and processed using the Nis-Elements AR software (Nikon). Images were analyzed using MicrobeJ, a plug-in of ImageJ (Ducret et

al., 2016). Data was analyzed in R and unless stated, represented as focus density maps plotted on the longitudinal axis of half cells ordered by cell length. Each spot represents the localization of an individual focus, and spot colour represents focus density at a specific location on the half cell. Cells with >0 foci shown for each time point. In cells possessing >1 foci, foci were represented adjacently on cells of the same length.

Western blots

To compare the expression profiles of competence proteins after competence induction, time course Western blots were carried out. Cells were diluted 100-fold in 10 mL C+Y medium pH 7 and grown to OD 0.1. Where appropriate, cells were induced with CSP (100 ng mL^{-1}) or BIP (250 ng mL^{-1}) peptide. At indicated time points, OD_{550} measurements were taken and 500 µL of culture was recovered. Samples were centrifuged (3 min, 3,000 g) and pellets were resuspended in 40 µL of TE 1x supplemented with 0.01% DOC and 0.02% SDS. Samples were then incubated for 10 minutes at 37°C before addition of 40 µL 2x sample buffer with 10% β-mercaptoethanol, followed by incubation at 85°C for 10 minutes. Samples were then normalized compared to the initial OD_{550} reading, and loaded onto SDS-PAGE gels (BIORAD). Samples were migrated for 30 min at 200V, and transferred onto nitrocellulose membrane using a Transblot Turbo (BIORAD). Membranes were blocked for 1h at room temperature in 1x TBS with 0.1% Tween20 and 10% milk, before two washes in 1x TBS with 0.1% Tween20 and probing with primary antibodies (1/10,000 as noted) in 1x TBS with 0.1% Tween20 and 5% milk overnight at 4°C. After a further four washes in 1x TBS with 0.1% Tween20, membranes were probes with anti-rabbit secondary antibody (1/10,000) for 1h 30 min, followed by another four washes in 1x TBS with 0.1% Tween20. Membranes were activated using Clarity Max ECL (BIORAD) and visualized in a ChemiDoc Touch (BIORAD).

Co-Immunoprecipitation

Co-immunoprecipitation was done using magnetic GFP-Trap beads as per manufacturer's instructions (Chromotek). Briefly, cells were inoculated 1/100 in 25 mL of C+Y medium pH 7 and grown to OD_{550} 0.1. Competence was induced by addition of 100 ng mL^{-1} CSP, and cells were incubated for 10 min at 37°C. Cultures were mixed with 25 mL cold buffer A (10 mM Tris pH 7.5, 150 mM NaCl) and centrifuged for 15 min at 5,000 g. Pellets were washed twice with 10 mL cold buffer A, and stored at -80°C until use. After defrosting, pellets were resuspended in 1 mL buffer B (10 mM Tris pH 7.5, 150 mM NaCl, 0.2mM EDTA, 0.1% TritonX100, 1 M DTT) and incubated for 10 minutes on ice, followed by 10 min at 37°C, and a further 10 min on ice. Samples were then sonicated (2 x 30s with 10s pause) and centrifuged for 30 min at 4°C and 16,000 g. After normalizing the protein concentrations in the samples, 20 µg mL^{-1} RNAse A and 50 µg mL^{-1} DNAse I were added and samples were tumbled end over end at 4°C for 30 min. 75 µl of GFP-Trap beads were added to the samples, which were then tumbled end over end at 4°C for 2 h 30 min. GFP-Trap beads were purified by magnetism and washed twice in 500 µL ice cold dilution buffer (10 mM Tris pH 7.5, 150 mM NaCl, 0.5mM EDTA), before being resuspended in 2x sample buffer + 10% β-mercaptoethanol and incubated at 95°C for 10 minutes. Samples were then run on SDS-PAGE gel and Western blots carried out as described above.

Pre-competence expression of DprA and σ^X.

Cells (R4500, CEPlac-dprA, dprA::spc, CEPIIR- R4509, R4511,) were grown to OD492 0.2 in 2 mL C+Y medium (pH7.6) with 50 µM IPTG. After centrifugation for 5 minutes at 5,000 rpm, cells were resuspended in 1 mL C+Y medium and stored at -80°C in 100 µL aliquots until required. Aliquots were resuspended in 900 µL fresh C+Y medium (pH7.6) and diluted 1/10 in a 96-ell plate in C+Y medium (pH 7.6) with luciferin and 50 µM IPTG to induce DprA expression. After 25 minutes, BIP (250ng $µL^{-1}$) was added where noted to induce σ^X. 20 minutes later, CSP (100ng $µL^{-1}$) was added to induce competence for 20 minutes. Luminometric and photometric reading were taken every 2 minutes during this time to report induction of *comC-luc*.

Acknowledgements

We thank Nathalie Campo and Mathieu Bergé for critical reading of the manuscript, and the rest of the Polard lab for helpful discussions. We thank Jérôme Rech for help creating Movies. We thank Jan-Willem Veening for kind donation of the pMK111 plasmid. This work was funded by the Agence Nationale de la Recherche (Grants ANR-10-BLAN-1331 and ANR-13-BSV8-0022).

Author Contributions

Conceptualization, C. J., M. P., P. P.; Methodology, C. J., P. P.; Investigation, C. J., A. L. S., M. B., M. P., D. D. L.; Writing – Original draft, C. J.; Writing – Review and editing, C. J., P. P.; Funding acquisition, P. P.

References

Aggarwal, S.D., Eutsey, R., West-Roberts, J., Domenech, A., Xu, W., Abdullah, I.T., Mitchell, A.P., Veening, J.-W., Yesilkaya, H., Hiller, N.L., 2018. Function of BriC peptide in the pneumococcal competence and virulence portfolio. PLoS Pathog. 14, e1007328. https://doi.org/10.1371/journal.ppat.1007328

Akerley, B.J., Rubin, E.J., Camilli, A., Lampe, D.J., Robertson, H.M., Mekalanos, J.J., 1998. Systematic identification of essential genes by in vitro mariner mutagenesis. Proc. Natl. Acad. Sci. U. S. A. 95, 8927–8932. https://doi.org/10.1073/pnas.95.15.8927

Alloing, G., Martin, B., Granadel, C., Claverys, J.P., 1998. Development of competence in Streptococcus pneumonaie: pheromone autoinduction and control of quorum sensing by the oligopeptide permease. Mol. Microbiol. 29, 75–83. https://doi.org/10.1046/j.1365-2958.1998.00904.x

Aprianto, R., Slager, J., Holsappel, S., Veening, J.-W., 2018a. High-resolution analysis of the pneumococcal transcriptome under a wide range of infection-relevant conditions. Nucleic Acids Res. 46, 9990–10006. https://doi.org/10.1093/nar/gky750

Aprianto, R., Slager, J., Holsappel, S., Veening, J.-W., 2018b. High-resolution analysis of the pneumococcal transcriptome under a wide range of infection-relevant conditions. Nucleic Acids Res. 46, 9990–10006. https://doi.org/10.1093/nar/gky750

Baker, M.D., Wolanin, P.M., Stock, J.B., 2006. Signal transduction in bacterial chemotaxis. BioEssays News Rev. Mol. Cell. Dev. Biol. 28, 9–22. https://doi.org/10.1002/bies.20343

Bergé, M., Moscoso, M., Prudhomme, M., Martin, B., Claverys, J.-P., 2002. Uptake of transforming DNA in Gram-positive bacteria: a view from Streptococcus pneumoniae. Mol. Microbiol. 45, 411–421.

Bergé, M.J., Kamgoué, A., Martin, B., Polard, P., Campo, N., Claverys, J.-P., 2013. Midcell recruitment of the DNA uptake and virulence nuclease, EndA, for pneumococcal transformation. PLoS Pathog. 9, e1003596. https://doi.org/10.1371/journal.ppat.1003596

Bergé, M.J., Mercy, C., Mortier-Barrière, I., VanNieuwenhze, M.S., Brun, Y.V., Grangeasse, C., Polard, P., Campo, N., 2017. A programmed cell division delay preserves genome integrity during

612 natural genetic transformation in Streptococcus pneumoniae. Nat. Commun. 8.
613 https://doi.org/10.1038/s41467-017-01716-9
614 Boyd, J.M., 2000. Localization of the histidine kinase PilS to the poles of Pseudomonas aeruginosa
615 and identification of a localization domain. Mol. Microbiol. 36, 153–162.
616 https://doi.org/10.1046/j.1365-2958.2000.01836.x
617 Caymaris, S., Bootsma, H.J., Martin, B., Hermans, P.W.M., Prudhomme, M., Claverys, J.-P., 2010. The
618 global nutritional regulator CodY is an essential protein in the human pathogen
619 Streptococcus pneumoniae. Mol. Microbiol. 78, 344–360.
620 Chastanet, A., Prudhomme, M., Claverys, J.P., Msadek, T., 2001. Regulation of Streptococcus
621 pneumoniae clp genes and their role in competence development and stress survival. J.
622 Bacteriol. 183, 7295–7307. https://doi.org/10.1128/JB.183.24.7295-7307.2001
623 Chen, J.D., Morrison, D.A., 1987. Modulation of competence for genetic transformation in
624 Streptococcus pneumoniae. J. Gen. Microbiol. 133, 1959–1967.
625 https://doi.org/10.1099/00221287-133-7-1959
626 Claverys, J.-P., Håvarstein, L.S., 2007. Cannibalism and fratricide: mechanisms and raisons d'être. Nat.
627 Rev. Microbiol. 5, 219–229. https://doi.org/10.1038/nrmicro1613
628 Claverys, J.-P., Prudhomme, M., Martin, B., 2006. Induction of competence regulons as a general
629 response to stress in gram-positive bacteria. Annu. Rev. Microbiol. 60, 451–475.
630 https://doi.org/10.1146/annurev.micro.60.080805.142139
631 Dagkessamanskaia, A., Moscoso, M., Hénard, V., Guiral, S., Overweg, K., Reuter, M., Martin, B., Wells,
632 J., Claverys, J.-P., 2004a. Interconnection of competence, stress and CiaR regulons in
633 Streptococcus pneumoniae: competence triggers stationary phase autolysis of ciaR mutant
634 cells. Mol. Microbiol. 51, 1071–1086.
635 Dagkessamanskaia, A., Moscoso, M., Hénard, V., Guiral, S., Overweg, K., Reuter, M., Martin, B., Wells,
636 J., Claverys, J.-P., 2004b. Interconnection of competence, stress and CiaR regulons in
637 Streptococcus pneumoniae: competence triggers stationary phase autolysis of ciaR mutant
638 cells. Mol. Microbiol. 51, 1071–1086.
639 Ducret, A., Quardokus, E.M., Brun, Y.V., 2016. MicrobeJ, a tool for high throughput bacterial cell
640 detection and quantitative analysis. Nat. Microbiol. 1, 16077.
641 https://doi.org/10.1038/nmicrobiol.2016.77
642 Fox, M.S., Hotchkiss, R.D., 1957. Initiation of bacterial transformation. Nature 179, 1322–1325.
643 https://doi.org/10.1038/1791322a0
644 Guiral, S., Mitchell, T.J., Martin, B., Claverys, J.-P., 2005. Competence-programmed predation of
645 noncompetent cells in the human pathogen Streptococcus pneumoniae: genetic
646 requirements. Proc. Natl. Acad. Sci. U. S. A. 102, 8710–8715.
647 https://doi.org/10.1073/pnas.0500879102
648 Håvarstein, L.S., Coomaraswamy, G., Morrison, D.A., 1995. An unmodified heptadecapeptide
649 pheromone induces competence for genetic transformation in Streptococcus pneumoniae.
650 Proc. Natl. Acad. Sci. U. S. A. 92, 11140–11144. https://doi.org/10.1073/pnas.92.24.11140
651 Hui, F.M., Zhou, L., Morrison, D.A., 1995. Competence for genetic transformation in Streptococcus
652 pneumoniae: organization of a regulatory locus with homology to two lactococcin A
653 secretion genes. Gene 153, 25–31. https://doi.org/10.1016/0378-1119(94)00841-f
654 Johnsborg, O., Kristiansen, P.E., Blomqvist, T., Håvarstein, L.S., 2006. A hydrophobic patch in the
655 competence-stimulating Peptide, a pneumococcal competence pheromone, is essential for
656 specificity and biological activity. J. Bacteriol. 188, 1744–1749.
657 https://doi.org/10.1128/JB.188.5.1744-1749.2006
658 Johnston, C., Hauser, C., Hermans, P.W.M., Martin, B., Polard, P., Bootsma, H.J., Claverys, J.-P., 2016.
659 Fine-tuning of choline metabolism is important for pneumococcal colonization. Mol.
660 Microbiol. 100, 972–988. https://doi.org/10.1111/mmi.13360
661 Johnston, C., Martin, B., Fichant, G., Polard, P., Claverys, J.-P., 2014. Bacterial transformation:
662 distribution, shared mechanisms and divergent control. Nat. Rev. Microbiol. 12, 181–196.
663 https://doi.org/10.1038/nrmicro3199

664 Johnston, C., Mortier-Barriere, I., Khemici, V., Polard, P., 2018. Fine-tuning cellular levels of DprA
665 ensures transformant fitness in the human pathogen Streptococcus pneumoniae. Mol.
666 Microbiol. 109, 663–675. https://doi.org/10.1111/mmi.14068
667 Kazmierczak, M.J., Wiedmann, M., Boor, K.J., 2005. Alternative sigma factors and their roles in
668 bacterial virulence. Microbiol. Mol. Biol. Rev. MMBR 69, 527–543.
669 https://doi.org/10.1128/MMBR.69.4.527-543.2005
670 Kloosterman, T.G., Hendriksen, W.T., Bijlsma, J.J.E., Bootsma, H.J., van Hijum, S.A.F.T., Kok, J.,
671 Hermans, P.W.M., Kuipers, O.P., 2006. Regulation of glutamine and glutamate metabolism by
672 GlnR and GlnA in Streptococcus pneumoniae. J. Biol. Chem. 281, 25097–25109.
673 https://doi.org/10.1074/jbc.M601661200
674 Lee, M.S., Morrison, D.A., 1999. Identification of a new regulator in Streptococcus pneumoniae
675 linking quorum sensing to competence for genetic transformation. J. Bacteriol. 181, 5004–
676 5016.
677 Lin, J., Lau, G.W., 2019. DprA-dependent exit from the competent state regulates multifaceted
678 Streptococcus pneumoniae virulence. Infect. Immun. https://doi.org/10.1128/IAI.00349-19
679 Lin, J., Zhu, L., Lau, G.W., 2016. Disentangling competence for genetic transformation and virulence in
680 Streptococcus pneumoniae. Curr. Genet. 62, 97–103. https://doi.org/10.1007/s00294-015-
681 0520-z
682 Luo, P., Li, H., Morrison, D.A., 2004. Identification of ComW as a new component in the regulation of
683 genetic transformation in Streptococcus pneumoniae. Mol. Microbiol. 54, 172–183.
684 https://doi.org/10.1111/j.1365-2958.2004.04254.x
685 Marie, L., Rapisarda, C., Morales, V., Bergé, M., Perry, T., Soulet, A.-L., Gruget, C., Remaut, H.,
686 Fronzes, R., Polard, P., 2017. Bacterial RadA is a DnaB-type helicase interacting with RecA to
687 promote bidirectional D-loop extension. Nat. Commun. 8, 15638.
688 https://doi.org/10.1038/ncomms15638
689 Martin, B., García, P., Castanié, M.P., Claverys, J.P., 1995. The recA gene of Streptococcus
690 pneumoniae is part of a competence-induced operon and controls lysogenic induction. Mol.
691 Microbiol. 15, 367–379.
692 Martin, B., Prats, H., Claverys, J.P., 1985. Cloning of the hexA mismatch-repair gene of Streptococcus
693 pneumoniae and identification of the product. Gene 34, 293–303.
694 https://doi.org/10.1016/0378-1119(85)90138-6
695 Martin, B., Prudhomme, M., Alloing, G., Granadel, C., Claverys, J.P., 2000. Cross-regulation of
696 competence pheromone production and export in the early control of transformation in
697 Streptococcus pneumoniae. Mol. Microbiol. 38, 867–878.
698 Martin, B., Soulet, A.-L., Mirouze, N., Prudhomme, M., Mortier-Barrière, I., Granadel, C., Noirot-Gros,
699 M.-F., Noirot, P., Polard, P., Claverys, J.-P., 2013. ComE/ComE~P interplay dictates activation
700 or extinction status of pneumococcal X-state (competence). Mol. Microbiol. 87, 394–411.
701 https://doi.org/10.1111/mmi.12104
702 Mirouze, N., Bergé, M.A., Soulet, A.-L., Mortier-Barrière, I., Quentin, Y., Fichant, G., Granadel, C.,
703 Noirot-Gros, M.-F., Noirot, P., Polard, P., Martin, B., Claverys, J.-P., 2013. Direct involvement
704 of DprA, the transformation-dedicated RecA loader, in the shut-off of pneumococcal
705 competence. Proc. Natl. Acad. Sci. U. S. A. 110, E1035-1044.
706 https://doi.org/10.1073/pnas.1219868110
707 Mortier-Barrière, I., Campo, N., Bergé, M.A., Prudhomme, M., Polard, P., 2019. Natural Genetic
708 Transformation: A Direct Route to Easy Insertion of Chimeric Genes into the Pneumococcal
709 Chromosome. Methods Mol. Biol. Clifton NJ 1968, 63–78. https://doi.org/10.1007/978-1-
710 4939-9199-0_6
711 Mortier-Barrière, I., de Saizieu, A., Claverys, J.P., Martin, B., 1998. Competence-specific induction of
712 recA is required for full recombination proficiency during transformation in Streptococcus
713 pneumoniae. Mol. Microbiol. 27, 159–170.
714 Mortier-Barrière, I., Velten, M., Dupaigne, P., Mirouze, N., Piétrement, O., McGovern, S., Fichant, G.,
715 Martin, B., Noirot, P., Le Cam, E., Polard, P., Claverys, J.-P., 2007. A key presynaptic role in

716 transformation for a widespread bacterial protein: DprA conveys incoming ssDNA to RecA.
717 Cell 130, 824–836. https://doi.org/10.1016/j.cell.2007.07.038
718 Österberg, S., del Peso-Santos, T., Shingler, V., 2011a. Regulation of alternative sigma factor use.
719 Annu. Rev. Microbiol. 65, 37–55. https://doi.org/10.1146/annurev.micro.112408.134219
720 Österberg, S., del Peso-Santos, T., Shingler, V., 2011b. Regulation of alternative sigma factor use.
721 Annu. Rev. Microbiol. 65, 37–55. https://doi.org/10.1146/annurev.micro.112408.134219
722 Pestova, E.V., Morrison, D.A., 1998. Isolation and characterization of three Streptococcus
723 pneumoniae transformation-specific loci by use of a lacZ reporter insertion vector. J.
724 Bacteriol. 180, 2701–2710.
725 Peterson, S.N., Sung, C.K., Cline, R., Desai, B.V., Snesrud, E.C., Luo, P., Walling, J., Li, H., Mintz, M.,
726 Tsegaye, G., Burr, P.C., Do, Y., Ahn, S., Gilbert, J., Fleischmann, R.D., Morrison, D.A., 2004.
727 Identification of competence pheromone responsive genes in Streptococcus pneumoniae by
728 use of DNA microarrays. Mol. Microbiol. 51, 1051–1070.
729 Pozzi, G., Masala, L., Iannelli, F., Manganelli, R., Havarstein, L.S., Piccoli, L., Simon, D., Morrison, D.A.,
730 1996. Competence for genetic transformation in encapsulated strains of Streptococcus
731 pneumoniae: two allelic variants of the peptide pheromone. J. Bacteriol. 178, 6087–6090.
732 https://doi.org/10.1128/jb.178.20.6087-6090.1996
733 Prudhomme, M., Attaiech, L., Sanchez, G., Martin, B., Claverys, J.-P., 2006. Antibiotic stress induces
734 genetic transformability in the human pathogen Streptococcus pneumoniae. Science 313,
735 89–92. https://doi.org/10.1126/science.1127912
736 Prudhomme, M., Claverys, J.-P., 2007. There will be a light: the use of luc transcriptional fusions in
737 living pneumococcal cells., in: The Molecular Biology of Streptococci. R. Hakenbeck, and G.S.
738 Chatwal, pp. 519–524.
739 Quevillon-Cheruel, S., Campo, N., Mirouze, N., Mortier-Barrière, I., Brooks, M.A., Boudes, M., Durand,
740 D., Soulet, A.-L., Lisboa, J., Noirot, P., Martin, B., van Tilbeurgh, H., Noirot-Gros, M.-F.,
741 Claverys, J.-P., Polard, P., 2012. Structure-function analysis of pneumococcal DprA protein
742 reveals that dimerization is crucial for loading RecA recombinase onto DNA during
743 transformation. Proc. Natl. Acad. Sci. U. S. A. 109, E2466-2475.
744 https://doi.org/10.1073/pnas.1205638109
745 Salles, C., Créancier, L., Claverys, J.P., Méjean, V., 1992. The high level streptomycin resistance gene
746 from Streptococcus pneumoniae is a homologue of the ribosomal protein S12 gene from
747 Escherichia coli. Nucleic Acids Res. 20, 6103. https://doi.org/10.1093/nar/20.22.6103
748 Sanchez-Puelles, J.M., Ronda, C., Garcia, J.L., Garcia, P., Lopez, R., Garcia, E., 1986. Searching for
749 autolysin functions. Characterization of a pneumococcal mutant deleted in the lytA gene.
750 Eur. J. Biochem. 158, 289–293. https://doi.org/10.1111/j.1432-1033.1986.tb09749.x
751 Slager, J., Aprianto, R., Veening, J.-W., 2019. Refining the Pneumococcal Competence Regulon by
752 RNA Sequencing. J. Bacteriol. 201. https://doi.org/10.1128/JB.00780-18
753 Slager, J., Kjos, M., Attaiech, L., Veening, J.-W., 2014. Antibiotic-induced replication stress triggers
754 bacterial competence by increasing gene dosage near the origin. Cell 157, 395–406.
755 https://doi.org/10.1016/j.cell.2014.01.068
756 Sung, C.K., Li, H., Claverys, J.P., Morrison, D.A., 2001. An rpsL cassette, janus, for gene replacement
757 through negative selection in Streptococcus pneumoniae. Appl. Environ. Microbiol. 67, 5190–
758 5196. https://doi.org/10.1128/AEM.67.11.5190-5196.2001
759 Sung, C.K., Morrison, D.A., 2005. Two distinct functions of ComW in stabilization and activation of the
760 alternative sigma factor ComX in Streptococcus pneumoniae. J. Bacteriol. 187, 3052–3061.
761 https://doi.org/10.1128/JB.187.9.3052-3061.2005
762 Tovpeko, Y., Bai, J., Morrison, D.A., 2016. Competence for Genetic Transformation in Streptococcus
763 pneumoniae: Mutations in σA Bypass the ComW Requirement for Late Gene Expression. J.
764 Bacteriol. 198, 2370–2378. https://doi.org/10.1128/JB.00354-16
765 van Raaphorst, R., Kjos, M., Veening, J.-W., 2017. Chromosome segregation drives division site
766 selection in Streptococcus pneumoniae. Proc. Natl. Acad. Sci. U. S. A. 114, E5959–E5968.
767 https://doi.org/10.1073/pnas.1620608114

768 Vidal, J.E., Howery, K.E., Ludewick, H.P., Nava, P., Klugman, K.P., 2013. Quorum-sensing systems
769 LuxS/autoinducer 2 and Com regulate Streptococcus pneumoniae biofilms in a bioreactor
770 with living cultures of human respiratory cells. Infect. Immun. 81, 1341–1353.
771 https://doi.org/10.1128/IAI.01096-12
772 Weng, L., Piotrowski, A., Morrison, D.A., 2013. Exit from competence for genetic transformation in
773 Streptococcus pneumoniae is regulated at multiple levels. PloS One 8, e64197.
774 https://doi.org/10.1371/journal.pone.0064197
775 Weyder, M., Prudhomme, M., Bergé, M., Polard, P., Fichant, G., 2018. Dynamic Modeling of
776 Streptococcus pneumoniae Competence Provides Regulatory Mechanistic Insights Into Its
777 Tight Temporal Regulation. Front. Microbiol. 9, 1637.
778 https://doi.org/10.3389/fmicb.2018.01637
779 Zhu, L., Lin, J., Kuang, Z., Vidal, J.E., Lau, G.W., 2015. Deletion analysis of Streptococcus pneumoniae
780 late competence genes distinguishes virulence determinants that are dependent or
781 independent of competence induction. Mol. Microbiol. 97, 151–165.
782 https://doi.org/10.1111/mmi.13016
783

784

785 **Figure Legends**

786 **Figure 1: DprA: Localization and roles in competence and transformation.**

787 (A) (1) Pre-CSP is exported and matured by the ComAB transporter, and then phosphorylates the
788 histidine kinase ComD. (2) ComD transphosphorylates ComE, which then stimulates the expression of
789 17 early *com* genes, including two copies of *comX*. (3) These encode an alternative sigma factor σ^X,
790 which controls late *com* genes including *dprA*. (4) DprA dimers load RecA onto ssDNA to mediate
791 transformation and interact with ComE~P to shut-off competence. (5) Transforming DNA is
792 internalized in single strand form and is protected from degradation by DprA and RecA (6), which then
793 mediate transformation (7). Orange arrows, early *com* promoters; purple arrows, late *com* promoters.
794 (B) Western blot tracking cellular levels of DprA-GFP after competence induction in strain R3728. α-
795 DprA antibody used. (C) Sample fluorescence microscopy images of R3728 strain producing DprA-GFP
796 15 minutes after competence induction. Scale bars, 1 μm. (D) Schematic representation of focus
797 density maps with half cells represented as vertical lines in ascending size order and localization of foci
798 represented along the length axis of each half cell. Black half-cells represent those presented, and grey
799 those not presented. (E) DprA-GFP accumulates at the cell poles during competence. 1290 cells and
800 1128 foci analyzed (F) Sample immunofluorescence microscopy images of a strain producing wildtype

DprA (R1502; wildtype) and a strain lacking DprA (R2018; *dprA*$^{-}$) fixed 15 minutes after competence induction. Scale bars, 1 µm.

Figure 2: Reducing cellular DprA-GFP levels results in loss of polar accumulation and competence shut-off

(A) Focus density maps of DprA-GFP foci at different cellular levels during competence. *CEP*$_{lac}$*-dprA-gfp* from strain R4262. Cellular DprA-GFP levels were controlled by growing cells in a gradient of IPTG. 1.5 µM IPTG, 11267 cells and 791 foci analyzed; 3 µM IPTG, 10623 cells and 748 foci analyzed; 6 µM IPTG, 10603 cells and 743 foci analyzed; 12.5 µM IPTG, 6985 cells and 1010 foci analyzed; 25 µM IPTG, 2945 cells and 1345 foci analyzed; 50 µM IPTG, 3678 cells and 1964 foci analyzed. Sample microscopy images of strain R4262 in varying IPTG concentrations. Scale bars, 1 µm. (B) Reducing cellular levels of DprA-GFP reduces the number of cells with foci. Error bars represent triplicate repeats. (C) Reducing cellular levels of DprA-GFP results specifically in loss of polar foci. Error bars represent triplicate repeats.

Figure 3: Analysis of the cellular localization of DprA-GFP

(A) DprA-GFP foci persist at the cell pole after competence shut-off Data at different time points after CSP addition represented as in Figure 1E. 4 minutes, 8336 cells and 1383 foci analyzed; 6 minutes, 2871 cells and 1674 foci analyzed; 10 minutes, 2614 cells and 1502 foci analyzed; 15 minutes, 1290 cells and 1128 foci analyzed; 20 minutes, 2110 cells and 1900 foci analyzed; 30 minutes, 789 cells and 831 foci analyzed; 60 minutes, 842 cells and 839 foci analyzed. Sample microscopy images of strain R3728 at varying times after competence induction. Scale bars, 1 µm. (B) Most competent cells possess a single polar focus of DprA-GFP. Error bars represent triplicate repeats. (C) Most cells possess polar DprA-GFP foci. Along the length of a cell of arbitrary length 1, polar foci are found between positions 0-0.15 and 0.85-1, midcell foci are found between 0.35 and 0.65, and anything in between is localized as betwixt. Error bars represent triplicate repeats.

Figure 4: Polar accumulation of DprA-GFP appears to depend on late *com* regulon expression

(A) Sample fluorescence microscopy images of strain R4060 producing DprA-GFP 15 minutes after induction with BIP or BIP and CSP. Scale bars, 1 µm. (B) Competence induction is required for optimal accumulation of DprA-GFP at the cell poles. Focus density maps as in Figure 1E. BIP+, 7845 cells and 790 foci analyzed; BIP+ CSP+, 2707 cells and 1478 foci analyzed. (C) Genetic context strain R4107 expressing *dprA-gfp* and only the late *com* regulon. P_{BIP} and P_X as in panel A, P_E represents early *com* promoter controlled by ComE. Light blue circle, ComW; light green oval, RNA polymerase; purple hexagon, σ^X. (D) Genetic context of strain R4140 expressing CEP_R-*dprA-gfp* and only the early *com* regulon. P_{BIP} as in panel A, P_E as in panel D. (E) Sample fluorescence microscopy images of strains producing DprA-GFP with only late (R4107) or only early (R4140) *com* operons 15 minutes after competence induction. Scale bars, 2 µm. (F) Induction of the late *com* regulon is required for accumulation of DprA-GFP at the cell poles. Focus density maps as in Figure 1E. 1988 cells and 1824 foci analyzed. (G) Focus density maps produced as in Figure 1E from images where DprA-GFP was produced outside of competence in presence or absence of σ^X. DprA-GFP alone, 7845 cells and 790 foci analyzed; DprA-GPF + σ^X, 3545 cells and 1355 foci analyzed. Strains used: DprA-GFP alone, R4060; DprA-GFP and σ^X, R4489.

Figure 5: σ^X-GFP interacts directly with DprA at the cell pole during competence

(A) Sample fluorescence microscopy images of strain R4451 producing σ^X-GFP from *comX1* and wildtype σ^X from *comX2* 15 minutes after competence induction. Scale bars, 1 µm. (B) σ^X-GFP accumulates at the cell poles during competence. Focus density maps presented as in Figure 1E. 4 minutes, 7544 cells and 489 foci analyzed; 6 minutes, 5442 cells and 1711 foci analyzed; 10 minutes, 4358 cells and 2691 foci analyzed; 15 minutes, 3746 cells and 2144 foci analyzed; 20 minutes, 4211 cells and 1754 foci analyzed; 30 minutes, 4695 cells and 1920 foci analyzed; 60 minutes, 5713 cells and 1016 foci analyzed. (C) Most cells have a single σ^X-GFP focus. Data from the time-course experiment presented in panel B showing the number of foci per cell at each time point. Error bars represent

853 triplicate repeats. (D) DprA-GFP foci persist in cells longer than σ^X-GFP foci. Comparison of cells with
854 foci at different timepoints from timecourse experiments. DprA-GFP from Figure 3A, σ^X-GFP from panel
855 B. Error bars represent triplicate repeats. (E) Accumulation of σ^X at the cell poles does not depend on
856 DprA. Sample microscopy images of a *comX1-gfp*, *dprA*$^-$ strain (R4469). Focus density maps generated
857 from cells visualized 15 minutes after competence induction presented as in Figure 1E. 1104 cells and
858 638 foci analyzed. (F) σ^X and DprA colocalize at the cell pole. Colocalization of σ^X-YFP and DprA-
859 mTurquoise in R4473 cells visualized 15 minutes after competence induction. 7460 cells and 3504
860 DprA-mTurquoise foci analyzed. Scale bars, 1 µm. (G) DprA is copurified with σ^X-GFP while DprA^{AR} is
861 not. Western blot of pull-down experiment carried out on strains producing σ^X-GFP and either DprA
862 (R4451) or DprA^{AR} (R4514) 10 minutes after competence induction. WCE, whole cell extract; FT1, flow
863 through; E, eluate.
864
865 **Figure 6: The main actors of competence induction and shut-off colocalize at the cell pole**
866 (A) Sample fluorescence microscopy images of cells producing ComE-GFP (R4010), GFP-ComD (R3914)
867 or wildtype cells (R1501) and *comD*$^-$ cells (R1745) exposed to CSP-HF. Scale bars, 1 µm. GFP-ComD,
868 1933 cells and 1397 foci; CSP-HF, 2105 cells and 2121 foci. (B) Focus density maps of cells producing
869 GFP-ComD (R3914) and wildtype (R1501) cells exposed to CSP-HF 15 minutes after competence
870 induction. Data presented as in Figure 1E. GFP-ComD, 1933 cells and 1397 foci analyzed; CSP-HF, 2105
871 cells and 2121 foci analyzed. (C) Number of foci present in cells possessing foci of different fluorescent
872 fusions 15 minutes after competence induction. Data taken from panel B except for DprA-GFP, taken
873 from Figure 3. (D) DprA-mTurquoise and ComE-YFP colocalization in competent R4176 cells visualized
874 by fluorescence microscopy 15 minutes after competence induction. 3143 cells and 2126 DprA-
875 mTurquoise foci analyzed. Scale bars, 1 µm. (E) DprA-mTurquoise and YFP-ComD colocalization in
876 competent R4111 cells visualized by fluorescence microscopy 15 minutes after competence induction.
877 2857 cells and 1335 DprA-mTurquoise foci analyzed. Scale bars, 1 µm. (F) DprA-GFP and CSP-HF

878 colocalization in competent R4062 cells visualized by fluorescence microscopy 15 minutes after
879 competence induction. 7588 cells and 3663 DprA-mTurquoise foci analyzed. Scale bars, 1 µm.
880
881 **Figure 7: Pre-competence expression of DprA and σ^X antagonizes competence induction**
882 (A) Inactivation of *comX1* or *comX2* does not impact transformation efficiency. Error bars represent
883 triplicate repeats. (B) Inactivation of *comX1* or *comX2* delays the shut-off of competence. Data is
884 plotted as Relative light units, corrected by optical density (RLU/OD) against OD. Error bars represent
885 triplicate repeats. (C) Visual representation of experiment exploring the impact of pre-competence
886 expression of DprA and σ^X on induction. (D) BIP induction of cells lacking $CEPII_R$-*comX* does not alter
887 competence induction. Cells possessing *comC-luc* and CEP_{lac}-*dprA* (R4511) were treated as described
888 in Panel C. Error bars represent triplicate repeats. (E) Production of σ^X and DprA prior to competence
889 induction antagonizes competence. Cells possessing *comC-luc* and CEP_{lac}-*dprA* and $CEPII_R$-*comX*
890 (R4500) were treated as in panel C. Error bars represent triplicate repeats. (F) Inactivation of *comW*
891 does not alter the antagonization of competence induction mediated by early DprA and σ^X production.
892 Cells possessing *comC-luc*, CEP_{lac}-*dprA*, $CEPII_R$-*comX* and *ΔcomW::trim* (R4509) were treated as in panel
893 C. Error bars represent triplicate repeats. (G) Polar competence induction in *Streptococcus*
894 *pneumoniae*. (1) Extracellular CSP interacts with ComD at the cell poles, prompting ComD
895 autophosphorylation. (2) Patches of ComE navigate around the cell membrane. (3) Polar ComD
896 phosphorylates ComE. (4) Active ComE~P dimers leave the cell poles to interact with genomic targets,
897 inducting the early *com* regulon and (5) launching an autocatalytic feedback loop. (6) Among the early
898 *com* genes, *comX1*, *comX2* and *comW* produce σ^X and its activator ComW, which induce the late *com*
899 regulon, including DprA. Orange arrows, early *com* promoters; purple arrows, late *com* promoters. C,
900 *comC*; D, *comD*; E, *comE*; X1/2, *comX1*/*comX2*; W, *comW*; RNAP, RNA polymerase. (H) Polar shut-off of
901 pneumococcal competence. (1) σ^X interacts directly with DprA, promoting accumulation of DprA at the
902 cell pole, generating a polar DprA 'cloud' in competent cells , near ComD (2). (3) Polar DprA interacts
903 directly with neosynthesized ComE~P, preventing the regulator from accessing its genomic targets. (4)

Unphosphorylated ComE interacts with early com promoters, acting as a repressor to prevent induction (Martin et al., 2013), promoting extinction of the competence signal, resulting in competence shut-off (5).

Supplementary Figure Legends

Figure S1: Validation of DprA-GFP activity

(A) Linear representation of DprA-GFP with the limits of Pfam02481 (in gray) and structural domains indicated. Interfaces of dimerization and interaction with RecA and ComE are indicated and represent the regions within which the majority of point mutations affecting interaction were identified (Mirouze et al., 2013; Quevillon-Cheruel et al., 2012). The GFP protein is separated from DprA by a linker, as described previously (Bergé et al., 2013). (B) Western blot tracking cellular levels of DprA-GFP after induction as shown from strains R4045 and R3728. α-DprA antibody used. Samples at each time point corrected by OD to render direct comparison of cellular levels possible. Full gel shows no degradation of DprA-GFP throughout growth. (C) DprA-GFP is active in transformation. Comparing transformation efficiency of wildtype (R1501), *drpA*$^{-}$ (R2018) and *dprA-gfp* (R3728) strains. R304 chromosomal DNA, conferring streptomycin resistance via *rpsL41* point mutation (Salles et al., 1992), used to transform at 1, 10 and 100 ng mL^{-1}. Error bars represent triplicate repeats. (D) DprA-GFP is partially active in competence shut-off. Comparing the competence profiles of wildtype (R1502), *drpA*$^{-}$ (R2018) and *dprA-gfp* (R3743) strains after CSP addition (100 ng mL^{-1}, t = 40 min). Luminometric and photometric readings of *ssbB-luc* transcriptional reporter fusion taken every 5 minutes. Full lines represent competence induction (RLU/OD) and dotted lines represent growth (OD). Error bars represent triplicate repeats. (E) Dimerization of DprA is necessary for accumulation of DprA-GFP at the cell poles. Western blot tracking cellular levels of DprA-GFP after competence induction in strain R4046. α-DprA antibody used. Samples at each time point corrected by OD to render direct comparison of cellular levels possible. In contrast to DprA-GFP (Figure 1B), the levels of DprA^{AR}-GFP continue to increase over

the time period of the experiment as competence is not shut-off in this DprA^{AR} strains (Quevillon-Cheruel et al., 2012). Sample fluorescence microscopy images of R4046 strain producing DprA^{AR}-GFP 15 minutes after competence induction. Scale bars, 1 µm. 1124 cells and 5 foci analyzed. (F) Disrupting the ability of DprA to interact with RecA (*dprA*^{QNQ}) does not impact the polar accumulation of DprA. Strain R4047 (*comC0, dprA*^{QNQ}*-gfp*) observed 15 minutes after competence induction. Data presented as in Figure 1E. 767 cells and 612 foci analyzed. Sample microscopy images of strain R4047 15 minutes after competence induction. Scale bars, 1 µm. (G) Inactivating the *comEC* transformation pore gene to prevent uptake of exogenous DNA does not impact the polar accumulation of DprA. Strain R4082 (*dprA-gfp, comEC*$^{-}$) observed 15 minutes after competence induction. Data presented as in Figure 1E, 632 cells and 778 foci analyzed. Sample microscopy images of strain R4082 15 minutes after competence induction. Scale bars, 1 µm. (H) Inactivation the recombinase gene *recA* to prevent homologous recombination does not impact the polar accumulation of DprA. Strain R4061 (*dprA-gfp, recA*$^{-}$) observed 15 minutes after competence induction. Data presented as in Figure 1E, 1393 cells and 996 foci analyzed. Sample microscopy images of strain R4061 15 minutes after competence induction. Scale bars, 1 µm. (I) DprA-GFP foci remain stable over time after competence induction. DprA-GFP foci tracked by time-lapse fluorescence microscopy every 5 minutes from 10 to 30 minutes after competence induction in strain R3728. Images analyzed by MicrobeJ (Ducret et al., 2016). Each series of linked spots represents a single focus tracked over time, localized in an averaged pneumococcal cell. (J) Sample time-lapse fluorescence microscopy images of strain R3728 used to generate panel H.

Figure S2: Validation of *CEP$_{lac}$-dprA-gfp* activity

(A) Western blots comparing cellular levels of DprA (R3833) and DprA-GFP (R4262) produced from the *CEP$_{lac}$* platform in cells lacking native *dprA* in varying concentrations of IPTG. α-DprA antibodies used. Samples at each IPTG concentration corrected by OD to render direct comparison of cellular levels possible. Cellular levels of DprA-GFP estimated from Western blots compared to purified DprA as previously described (Johnston et al., 2018). (B) Transformation efficiency of a *CEP$_{lac}$-dprA-gfp*, *dprA*$^{-}$

strain (R4262) in an IPTG concentration gradient. R304 chromosomal DNA (50 ng mL^{-1}), conferring streptomycin resistance via *rpsL41* point mutation (Salles et al., 1992), used to transform. Error bars represent triplicate repeats. (C) Competence profiles of a R4262 strain possessing *CEP_{lac}-dprA-gfp* and *ssbB-luc* in an IPTG concentration gradient. Appropriate IPTG concentration present from the beginning of the culture. Competence induced by addition of CSP at t=0, when OD = ~0.05. Plots representative of triplicate repeats.

Figure S3: Validation of strains expressing *CEP_R-dprA-gfp* and the late *com* regulon alone

(A) Western blots tracking cellular levels of DprA-GFP in R4060 (*CEP_R-dprA-gfp dprA$^-$*), R4088 (*dprA-gfp CEP_R-comXW*) and R4140 (*CEP_R-dprA-gfp comX12$^-$ comW$^-$*) strains after induction with BIP. Either α-GFP or α-DprA antibodies used. Samples at each timepoint corrected by OD to render direct comparison of cellular levels possible. (B) Comparing transformation efficiencies of isogenic strains impaired for competence auto-induction. R1501 ("wildtype"), R2018 (*dprA$^-$*), R4060 (*CEP_R-dprA-gfp dprA$^-$*) and R4088 (*dprA-gfp CEP_R-comXW*) strains after induction with either CSP, BIP or both, as shown. *rpsL41* PCR fragment, conferring streptomycin via point mutation (Salles et al., 1992), used to transform at 50 ng mL^{-1}. Error bars represent triplicate repeats. (C) Exploring the competence profile of a strain ectopically expressing DprA-GFP under the control of BIP. R1501 (wildtype), R2018 (*dprA$^-$*) and R4060 (*CEP_R-dprA-gfp dprA$^-$*) strains. Experiment carried out as as in Figure S1D. Error bars represent triplicate repeats. (D) Exploring the competence profile of a strain ectopically expressing σ^X and ComW under the control of BIP and DprA-GFP from its native promoter. R1501 (wildtype), R2018 (*dprA$^-$*) and R4088 (*CEP_R-comXW, dprA-gfp, cbpD::cat*) strains. Experiment carried out as as in Figure S1D. Error bars represent triplicate repeats.

Figure S4: σ^X is necessary and sufficient to mediate accumulation of DprA at the cell poles.

(A) DprA-GFP accumulates at the cell poles in the absence of ComW. Localization of DprA-GFP in R4168 strain (*dprA-gfp*, *rpoD*^{A171V}, *comW*$^{-}$) 15 minutes after competence induction. Sample fluorescence microscopy images shown. Scale bars, 1 µm. Focus density maps presented as in Figure 3B. 3592 cells and 2101 foci analyzed. (B) Production of σ^X outside of competence promotes accumulation of DprA-GFP at the cell poles. Sample fluorescence microscopy images of cells producing DprA-GFP (R4060) or DprA-GFP and σ^X (R4489) outside of competence. Focus density maps presented as in Figure 3B. DprA-GPF + σ^X, 3545 cells and 1355 foci analyzed. *CEP*$_R$*-dprA-gfp* induced by BIP, 7845 cells and 790 foci analyzed; *CEP*$_R$*-dprA-gfp* induced by BIP and CSP, 5889 cells and 2254 foci analyzed; *CEP*$_R$*-dprA-gfp, CEPIIR-comX* induced by BIP, 3545 cells and 1355 foci analyzed; *CEP*$_R$*-dprA-gfp, CEPIIR-comX* induced by BIP and CSP, 6085 cells and 2458 foci analyzed. Scale bars, 1 µm. (C) Data from analysis of images in panel A split into cells with 0, 1 or 2 foci. (D) Western blot comparing expression of late *com* regulon by tracking cellular levels of SsbB in R1501 (wildtype) and R4509 (*CEPII*$_R$*-comX, comW*$^{-}$) strains. R1501 induced by CSP at t=0 and R4509 induced by BIP. Samples at each time point corrected by OD to render direct comparison of cellular levels possible. Relative SsbB levels measured by quantifying SsbB bands and normalizing to the band of SsbB expression 10 minute after BIP addition to R4509 as 1. α-σ^X and α-SsbB antibodies used as shown.

Figure S5: Validation of *comW* and *comX* fluorescent fusions

(A) ComW-GFP is diffuse within the cell cytoplasm. Localization of ComW-GFP in R4513 strain (*comW-gfp*, *comW*$^{+}$) 15 minutes after competence induction. Sample fluorescence microscopy images shown. Scale bars, 2 µM. Focus density maps presented as in Figure 1E. 9705 cells and 701 foci analyzed. (B) Western blots showing expression of ComW, ComW-GFP, SsbA and SsbB in response to CSP addition to either R1501 (wildtype) or R4513 (*comW-gfp*, *comW*$^{+}$) cells. α-ComW or α-SsbB antibodies used as shown. α-SsbB antibodies recognize both SsbA and SsbB. Samples at each time point corrected by OD to render direct comparison of cellular levels possible. (C) Western blots tracking cellular levels of σ^X, σ^X-GFP and DprA after competence induction in R4451 (*comX1-gfp*) and R4461 (*comX1-gfp*, *comX2*$^{-}$)

strains. α-σ^X and α-DprA antibodies used as shown. Samples at each time point corrected by OD to render direct comparison of cellular levels possible. (D) σ^X-GFP is partially active in competence induction. Comparing the competence profiles of R1502 (*ssbB-luc*), R4471 (*comX1-gfp, ssbB-luc*) and R4465 (*comX1-gfp*, *comX2*$^-$*, ssbB-luc*) strains. Data presented as described in Figure S1D. Error bars represent triplicate repeats. (E) Comparing transformation efficiencies of R1501 (wildtype), R4451 (*comX1-gfp*) and R4461 (*comX1-gfp*, *comX2*$^-$) strains. *rpsL41* PCR fragment, conferring streptomycin via point mutation (Salles et al., 1992), used to transform at 50 ng mL^{-1}. Error bars represent triplicate repeats. (F) σ^X-GFP is active in the shut-off of competence. Comparison of competence profiles of R1502 (*ssbB-luc*), R4471 (*comX1-gfp, ssbB-luc*) and R4466 (*comX1*$^-$ *ssbB-luc*) strains as described in Figure S1D. Comparison of data from panel E and Figure 7B. Error bars represent triplicate repeats.

Figure S6: Validation of ComE-GFP, GFP-ComD and CSP-HF

(A) ComE-GFP and GFP-ComD are produced stably after induction of competence. Western blots tracking cellular levels of ComE-GFP (R4010) and GFP-ComD (R3914) after induction of competence. α-ComD and α-ComE antibodies used. Samples corrected by OD to render direct comparison of cellular levels possible. (B) Western blot comparing ComE-GFP (R4010) and ComE (R1501) 15 minutes after competence induction, showing that ComE-GFP is not degraded. (C) Western blot comparing GFP-ComD (R3914) and ComD (R1501) 15 minutes after competence induction, showing that GFP-ComD is not degraded. (D) Comparison of competence induction profiles of R1502 (*ssbB-luc*), R4087 (*comE-gfp, ssbB-luc*) and R3915 (*gfp-comD, ssbB-luc*) strains as described in Figure S1D. Error bars represent triplicate repeats. (E) Comparison of transformation efficiencies at varying time points after competence induction in R1501 (wildtype), R4010 (*comE-gfp*) and R3914 (*gfp-comD*) strains. R304 chromosomal DNA (50 ng mL^{-1}), conferring streptomycin resistance via *rpsL41* point mutation (Salles et al., 1992), used to transform at indicated time points. (F) Comparison of competence induction profiles of concentration gradients of CSP and CSP-HF. Strain used, R1501 (*ssbB-luc*) Luminometric

readings taken every 30 seconds during the experiment. (G) ComD localizes to the cell pole in the absence of the late *com* regulon. Focus density maps of strain R4916 (*gfp-comD*, *comX1*$^{-}$, *comX2*$^{-}$, *comW*$^{-}$) 15 minutes after competence induction presented as in Figure 1E. Sample microscopy images of strain R4196 15 minutes after competence induction. Scale bars, 1 µm.

Figure S7: Time-course experiments tracking the localization of ComE-GFP, GFP-ComD and CSP-HF after competence induction

(A) ComE-GFP forms patches around the cell membrane in competent cells. Sample microscopy images of strain R4010 at varying time points after competence induction. Scale bars, 1 µm. (B) GFP-ComD accumulates at the cell poles in competent cells. Focus density maps of GFP-ComD (R3914) in time-course experiment after competence induction. Data presented as in Figure 1E. 4 minutes, 18772 cells and 832 foci analyzed; 6 minutes, 2115 cells and 770 foci analyzed; 10 minutes, 1581 cells and 944 foci analyzed; 15 minutes, 1933 cells and 1397 foci analyzed; 20 minutes, 2549 cells and 2311 foci analyzed; 30 minutes, 2526 cells and 2299 foci analyzed; 60 minutes, 3358 cells and 2428 foci analyzed. Sample microscopy images of strain R3914 at varying time points after competence induction. Scale bars, 1 µm. (C) CSP-HF accumulates at the cell poles in competent cells. Focus density maps of CSP-HF in time-course experiment after competence induction of R1501 strain. Data presented as in Figure 1E. 4 minutes, 2928 cells and 1671 foci analyzed; 6 minutes, 2581 cells and 2283 foci analyzed; 10 minutes, 2391 cells and 2795 foci analyzed; 15 minutes, 2105 cells and 2121 foci analyzed; 20 minutes, 1279 cells and 2515 foci analyzed; 30 minutes, 1997 cells and 2052 foci analyzed; 60 minutes, 993 cells and 735 foci analyzed. Sample microscopy images of strain R1501 at varying time points after competence induction. Scale bars, 1 µm.

Supplementary Materials and Methods

Strain construction

Here we describe how the new plasmids and mutants used in this study were generated. Previously published constructs and mutants were simply transferred from published strains by transformation with appropriate selection. The pMB42 plasmid was generated by amplifying *gfp* with primer pair OMB4-OMB5 and the 5' end of *dprA* with primer pair dprA22-dprA23. The resulting DNA fragments were digested by *Xho*I/*Hind*III and *Xho*I/*Eco*RI respectively, and both ligated into a pUC59-derived plasmid pAO-0 plasmid digested with *Eco*RI and *Hind*III. This generated a plasmid which, when transformed into pneumococci, generated a strain possessing *dprA-gfp* at the native locus, as well as a *spc* resistance cassette. A strain containing *dprA-gfp* at the native *dprA* locus (R3728) was constructed by transforming R1501 (*comC0*) with the pMB42 plasmid and selecting for spectinomycin resistance. To generate the pMB42-dprA^{AR} and pMB42-dprA^{QNQ} plasmids, the same primer pair was used to amplify *dprA* from strains R2585 and R2830, and the plasmids were generated in the same manner. These plasmids were transformed into R1501 (*comC0*) to generate R4046 and R4047 respectively. To generate pMB42-mKate2, mKate2 was amplified by PCR using the pMK111 plasmid as a template with primer pair CJ431-CJ432. pMB42 plasmid and the resulting PCR product were digested with *Xho*I and *Hind*III restriction enzymes, and ligated together to generate pMB42-mKate2. pMB42-mTurquoise was generated in the same manner using R4011 as template and the CJ454-CJ455 primer pair. These plasmids were transformed into R1501 (*comC0*) to generate R4048 and R4062 respectively.

To generate a strain possessing *comX1-gfp*, a DNA fragment comprising the *gfp* gene flanked by 5' and 3' regions of the *comX1* gene was generated by splicing overlap extension (SOE) PCR. The primer pairs used to generate the 5' *comX1* region, *gfp* and the 3' *comX1* region were respectively CJ643-CJ644, CJ645-CJ646 and CJ647-CJ648, using R3728 genomic DNA as a template. The resulting PCR fragments were fused by SOE PCR and transformed into R1501 (*comC0*) without selection. 100 clones were screened by PCR with the primer pair CJ643-CJ648 to identify *comX1-gfp* clones, one of which was named R4451. To generate a strain possessing *comE-gfp*, the same method was used with the primer pairs CJ379-CJ380, CJ381-CJ382, CJ383-CJ384 to generate the individual fragments and CJ379-CJ384 to generate the SOE fragment. To generate a strain possessing *comW-gfp*, the same

method was used with the primer pairs CJ508-CJ514, CJ515-CJ516, CJ517-CJ513 to generate the individual fragments and CJ508-CJ513 to generate the SOE fragment. To generate *gfp-comD*, PCR fragments of the regions up and downstream of the *comD* start codon and *gfp*, by PCR on R3728 with primer pairs MP216-MP217, MP220-MP221 and MP218-MP218 respectively. SOE PCR on these three fragments using primer pair MP216-MP221 generated *gfp-comD* with flanking sequences. This fragment was transformed into R1036 (*rpsL1, ΔcomC::kan-rpsL*), which contains a Janus cassette in the *comCDE* locus (Sung et al., 2001), with streptomycin selection, to replace the Janus cassette as previously described (Sung et al., 2001). To generate the plasmid pCEP$_R$-dprA-gfp, *dprA-gfp* was amplified from R3728 using primer pair CJ410-CJ411, possessing restriction sites *Nco*I and *Bam*HI respectively. This fragment and the pCEP$_R$-luc (Johnston et al., 2016) plasmid were digested and ligated together to generate pCEP$_R$-dprA-gfp. This plasmid was transformed into R1501 (*comC0*) with kanamycin selection to generate R4045. For each fluorescent fusion, a LEGSG linker was placed between *gfp* and the gene as previously described (Bergé et al., 2013).

To inactivate the 18 *cin* boxes of each late *com* operon individually, two PCR fragments were generated for each with homology to the 5' and 3' regions flanking the *cin* boxes using primers DDL48 to DDL121 (See Table S3 for details), with the entire 8 bp *cin* box (TACGATAA, (Lee and Morrison, 1999) replaced with a *Bam*HI site and two flanking base pairs as shown (A*GGATCC*T). In some cases, the first and last bases were altered so as not to match those of a particular *cin box* sequence (Table S3). SOE PCR using the flanking primers for each *cin* box (eg. DDL64 and DDL67 for *dprA*$^{cinbox-}$) generated a single fragment of ~2,500 bp with the mutated *cin* box flanked by ~1,250 bp of homology on either side. These SOE PCR fragments were individually transformed into R4431 (*comC0, radA-gfp, dprA-mKate2*), and 20 clones were picked for each transformation. The *radA-gfp* construct was present in this strain as part of another study and will not be discussed here, but explains why the *dprA-mKate2* fusion was used here. The targeted *cin* box sites were amplified by PCR on 10 clones in each case, using the same primers as for the SOE PCR, then digested by *Bam*HI and screened on agarose gel (1%). Mutated clones

were identified as those whose amplified PCR fragment was digested by *Bam*HI, indicating insertion of the transforming DNA fragment and resulting *cin* box mutation.

To generate the pCEP$_{lac}$-dprA-gfp plasmid, *P$_{syn}$-lacI-P$_{lac}$-dprA* and *P$_{syn}$-kan-treR* fragments were amplified from the CEP platform in strain R3833 using primer pairs AmiF1-CJ496 and CJ499-CJ500, while *gfp* was amplified from R3728 using primer pair CJ497-CJ498. These three fragments were used to generate a large *CEP$_{lac}$-dprA-gfp* SOE PCR fragment using primer pair AmiF1-CJ500, possessing the entire *CEP$_{lac}$-dprA-gfp* platform as well as flanking sequence, which was then transformed into R1501 (*comC0*) with kanamycin selection to generate R4261.

To delete *comW* and replace it with a trimethoprim resistance cassette, the sequences 5' and 3' of the *comW* gene were amplified using primer pairs CJ559-CJ560 and CJ563-CJ564, and the *trim* resistance cassette was amplified from strain TK108 (Kloosterman et al., 2006) by primer pair CJ561-CJ562. These three fragments were fused by SOE PCR with the primer pair CJ559-CJ564 and the resulting fragment was transformed into R1501 (*comC0*) to generate R4575 (*comC0, ΔcomW::trim*). To delete the entire *comCDE* operon and replace it with a trimethoprim resistance cassette, the sequences 5' and 3' of the *comW* gene were amplified using primer pairs CJ385-CJ470 and CJ473-CJ384, and the *trim* resistance cassette was amplified from strain TK108 (Kloosterman et al., 2006) by primer pair CJ471-CJ472. These three fragments were fused by SOE PCR with primer pair CJ385-CJ384 and the resulting fragment was transformed into R1501 (*comC0*) to generate R4574 (*ΔcomCDE::trim*).

Pre-competence expression of DprA and σ^X

To test whether pre-competence expression of DprA and σ^X antagonized competence induction, we generated strains which possessed an ectopic platform expressing *dprA* in response to IPTG (*CEP$_{lac}$-dprA*) (Johnston et al., 2018) alone or in addition to an ectopic platform expressing *comX* in response to the BIP peptide (*CEPII$_R$-comX*). We showed previously that ectopic expression of *dprA-gfp* and *comX* resulted in localization of DprA-GFP to the cell poles, unlike ectopic expression of *dprA-gfp* alone (Figure 5A). In the present experiment, expression of *dprA* was induced throughout growth by the

presence of 50µM IPTG in the culture medium. Cells were grown to OD_{550} 0.08, and were either exposed to BIP to induce *comX*, or not. Twenty minutes after this, CSP was added to the culture to induce competence, and the induction of the early *com* regulon was tracked by measuring activity of a *comC-luc* transcriptional reporter fusion (Bergé et al., 2002) every 2 minutes for 20 minutes to observe initial competence induction.

Supplementary Results

Assessing the activity of DprA-GFP

To determine the functionality of a DprA-GFP fluorescent fusion, we compared the transformation and competence shut-off of this strain to wildtype and *dprA*$^-$ controls. DprA-GFP displayed near wildtype activity in transformation and competence shut-off measured using an *ssbB-luc* transcriptional reporter fusion (Figure S1CD) as previously described (Prudhomme and Claverys, 2007).

Construction and validation of strains expressing only early or late com *regulons*

To express only the late *com* regulon, the *comX* and *comW* genes were placed under the control of BIP at the CEP expression platform (Weyder et al., 2018) in a strain possessing *dprA-gfp* at the native locus, with the *comCDE* operon deleted to prevent any expression of early *com* operons (Figure 4C). In addition, the *cbpD* gene was inactivate to compensate for the absence of the early com gene *comM*(Bergé et al., 2017; Guiral et al., 2005). Addition of BIP to this strain resulted in induction of the late *com* regulon in the absence of the autocatalytic feedback loop generated by the early *com* regulon. This strain transformed equally well upon CSP or BIP addition, showing that late *com* regulon expression is sufficient for transformation (Figure S3B). However, since the catalytic feedback loop of the early *com* genes was removed, little to no shut-off of late *com* gene expression was observed (Figure S3D). To express only the early *com* regulon, both copies of *comX*, along with *comW*, were

inactivated in a strain possessing *CEP_R-dprA-gfp* (Figure 4D). Addition of both BIP and CSP to this strain resulted in the induction of the early *com* regulon and the production of DprA-GFP. Since no other late *com* genes were expressed in this strain, the strain could not transform and the induction profile of *ssbB-luc* could not be tracked.

Validation of successful* cin box *inactivation

Successful *cin box* inactivation was confirmed in three individual *cin box* mutants with known transformation deficits, and each strain displayed the expected transformation deficit (Table S1), showing that as expected, full *cin box* mutation successfully abrogated σ^X-mediated expression, and allowing extrapolation to the 18 *cin box* mutants generated.

Assessing the activity of σ^X-GFP

In the absence of *comX2*, the second gene producing σ^X, σ^X-GFP induced the late *com* regulon poorly and was thus weakly transformable (Figure S5CDE). As a result, a strain possessing *comX1-gfp* and *comX2* was used to determine the localization of σ^X -GFP. This strain developed competence at a level only slightly lower than wild-type and transformed at wildtype levels (Figure S5DE). In addition, comparing competence profiles of *comX1*$^-$ and *comX1-gfp* showed that a strain producing σ^X from *comX2* and σ^X-GFP from *comX1*, shut-off competence more efficiently than a strain producing only σ^X from *comX2* (Figure S5F), suggesting that although σ^X-GFP is weakly active for competence induction, it is functional for its role in competence shut-off at the cell poles.

Assessing the activity of ComE-GFP, GFP-ComD and CSP-HF

1178 ComE-GFP was fully functional in competence induction and resulting transformation efficiency, while
1179 GFP-ComD displayed a delayed, weaker induction of competence, mimicked by transformation
1180 efficiency (Figure S6DE). Induction of competence with CSP-HF displayed a slight delay compared to
1181 wildtype CSP, and although induction levels were similar at high concentrations, lower concentrations
1182 of CSP-HF induced competence less than wildtype (Figure S6F). Nonetheless, the full or partial
1183 functionality of these fusion proteins allowed exploration of their localization in competent cells

1184

1185 **Table S3 refs:** (Akerley et al., 1998; Caymaris et al., 2010; Marie et al., 2017; Martin et al., 1995, 1985;
1186 Mortier-Barrière et al., 2019; Sanchez-Puelles et al., 1986; van Raaphorst et al., 2017)

1187

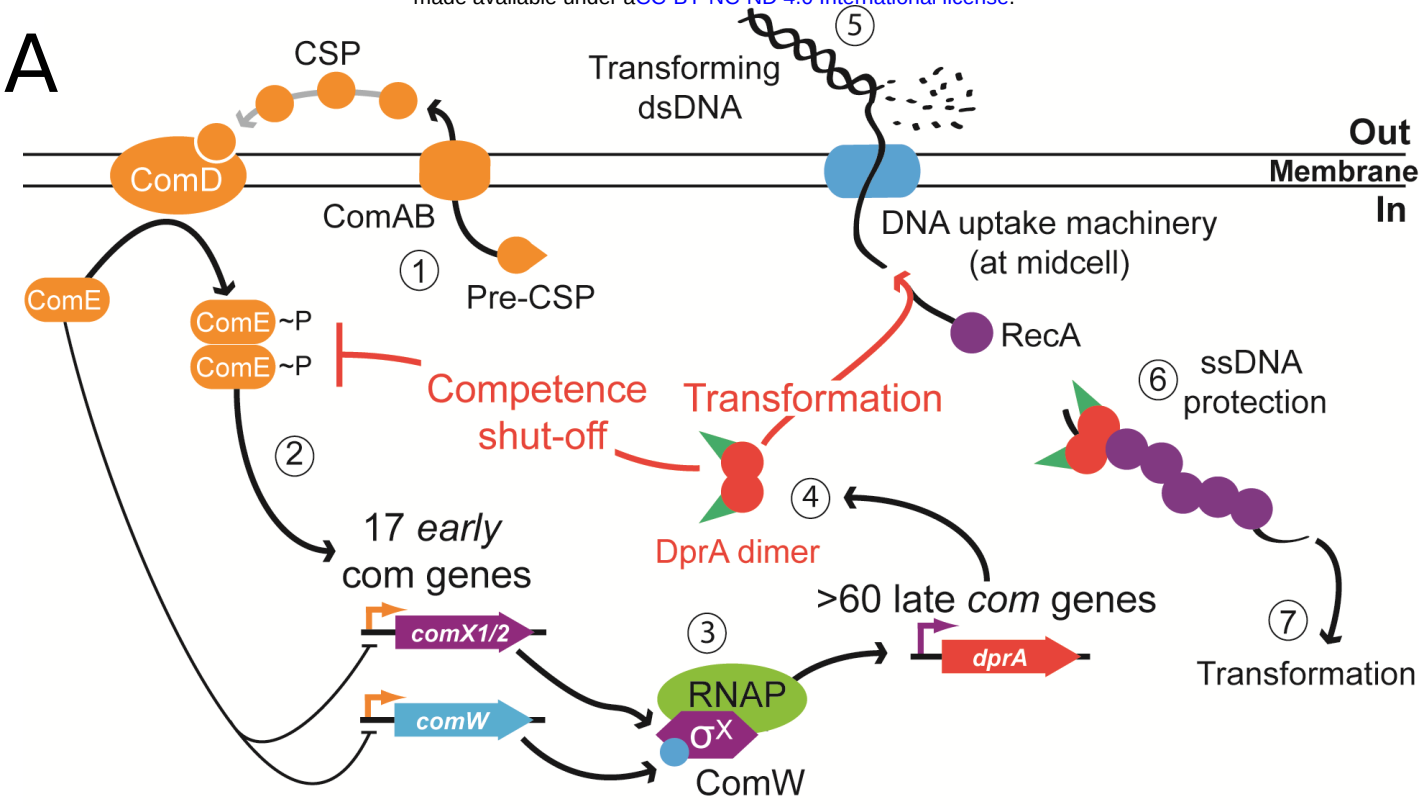

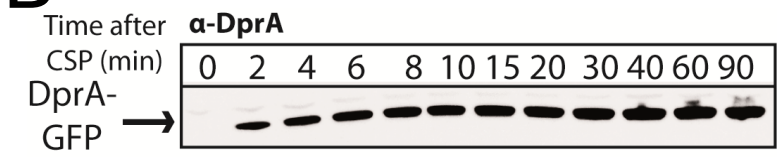

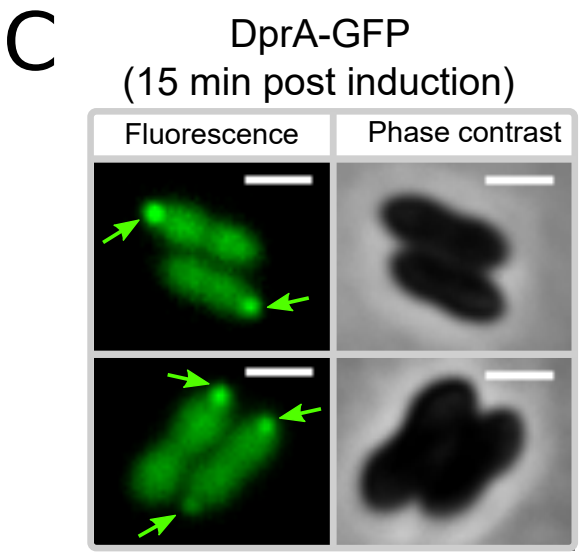

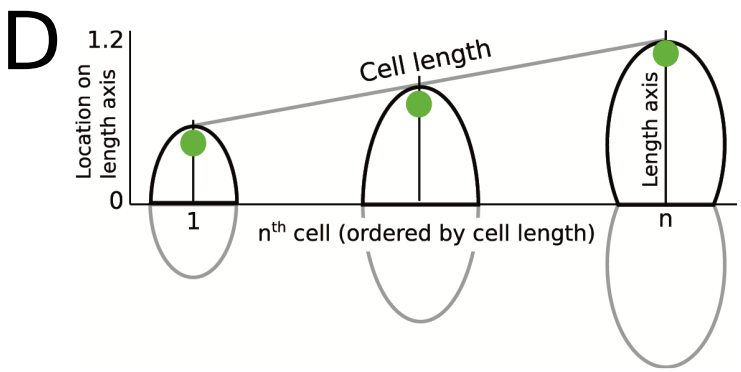

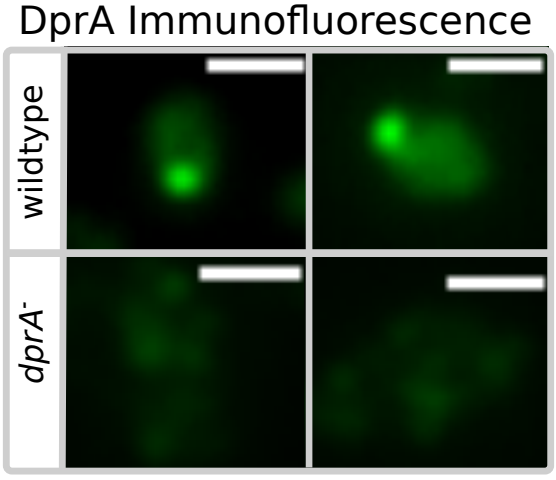

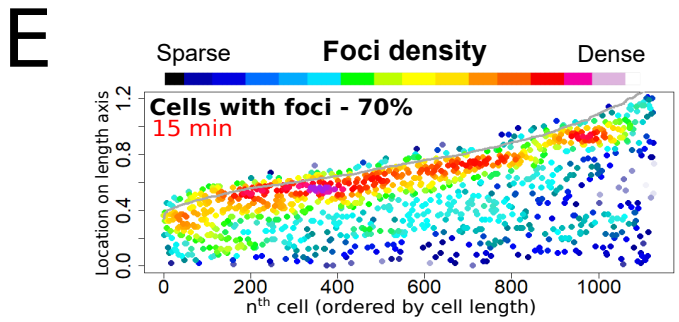

Figure 1

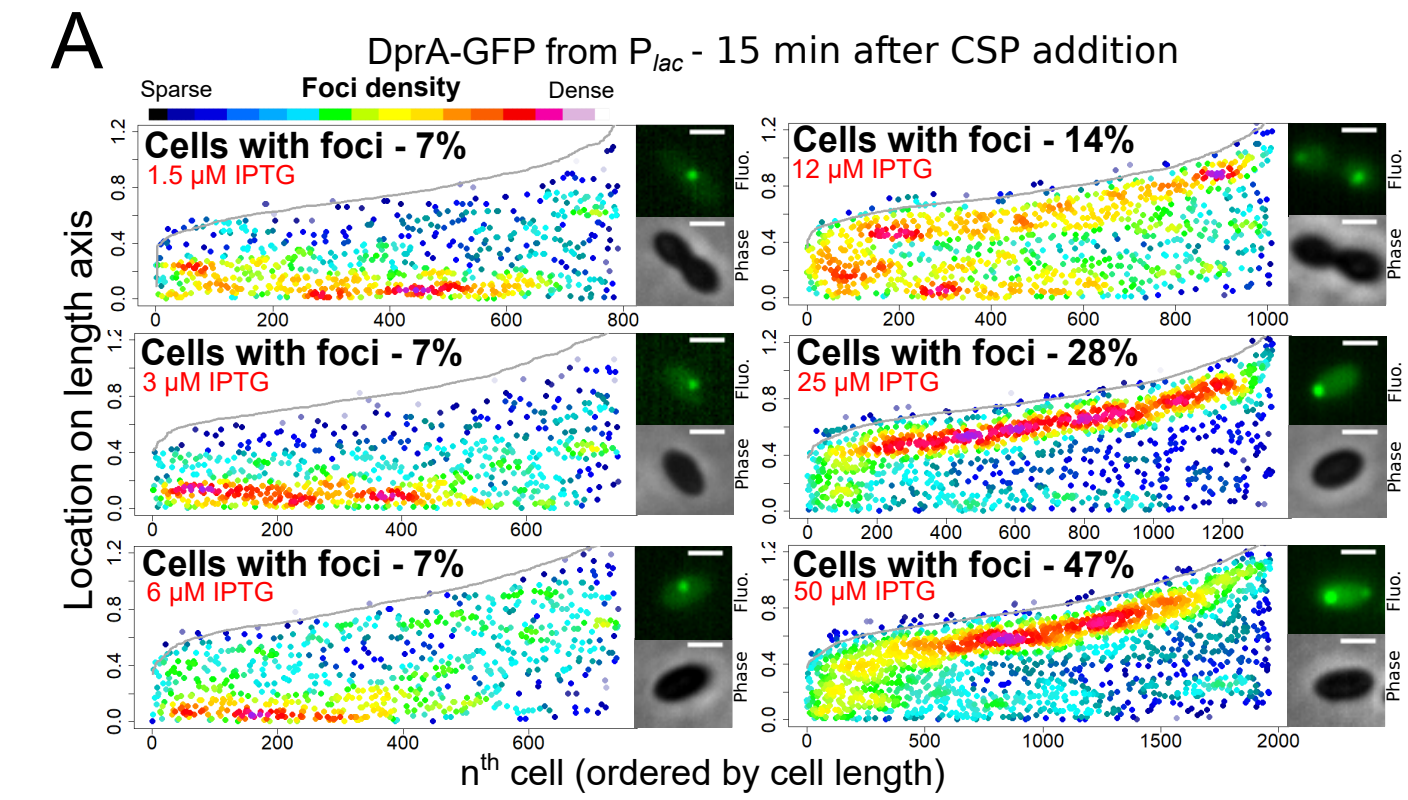

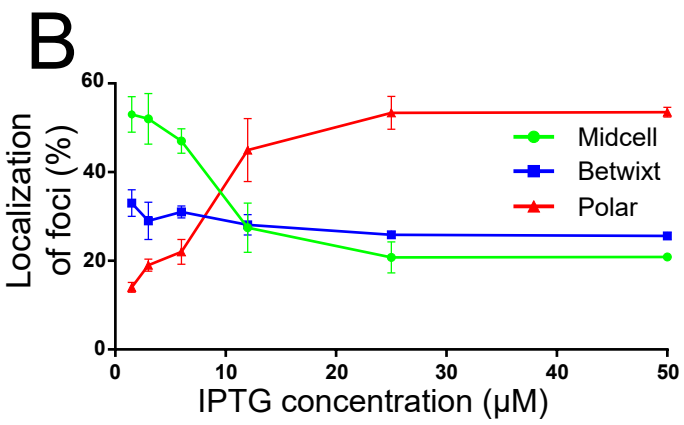

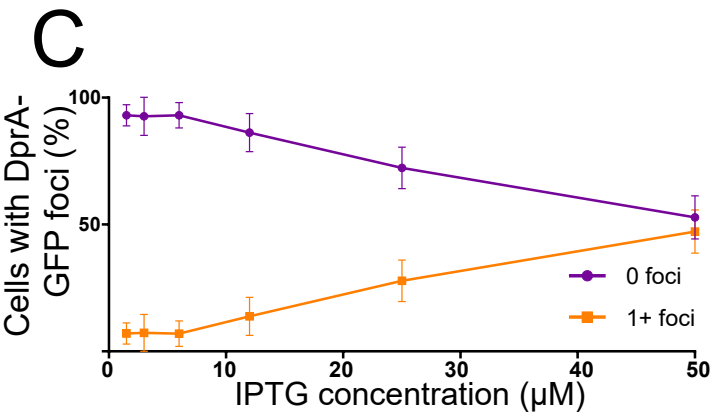

Figure 2

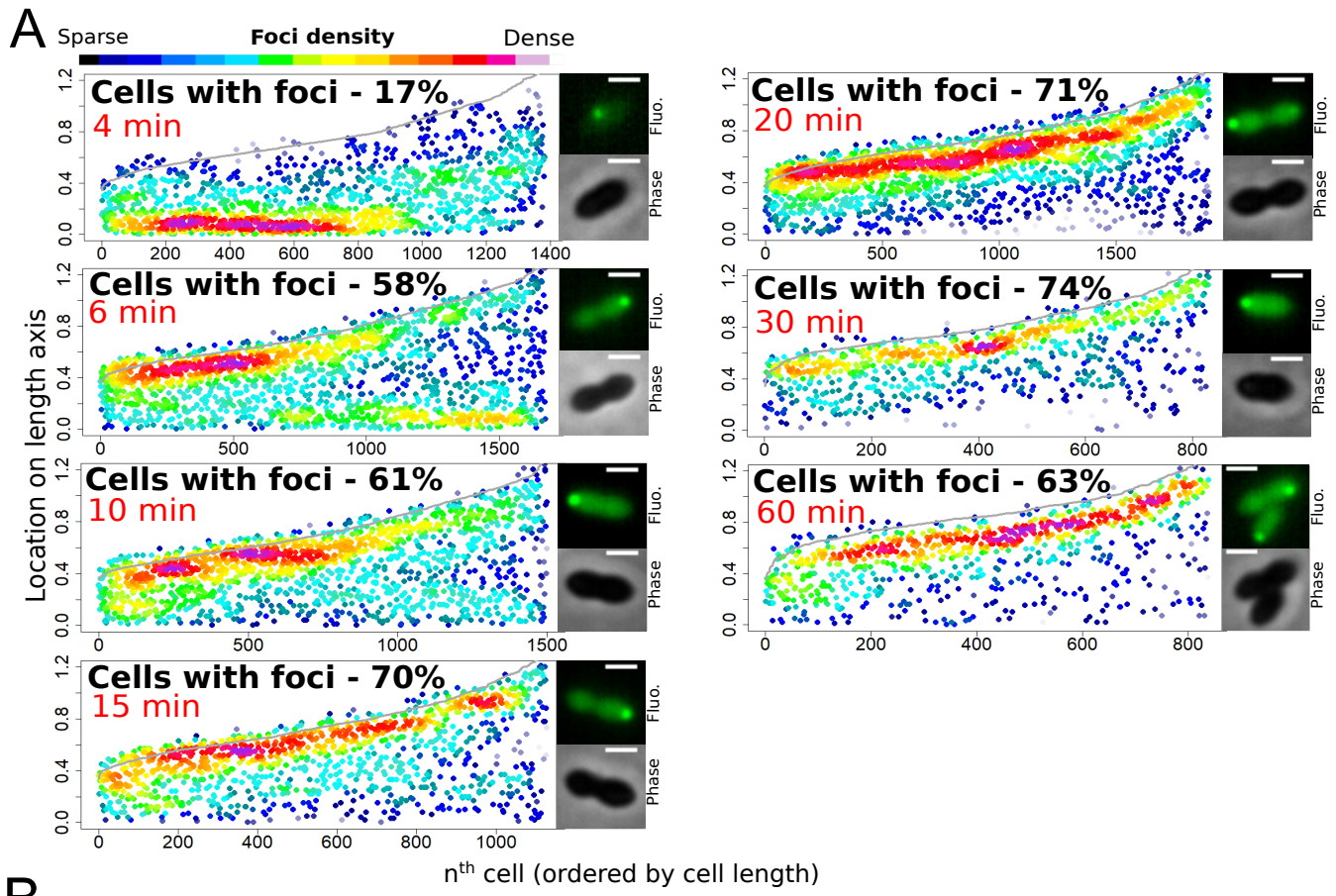

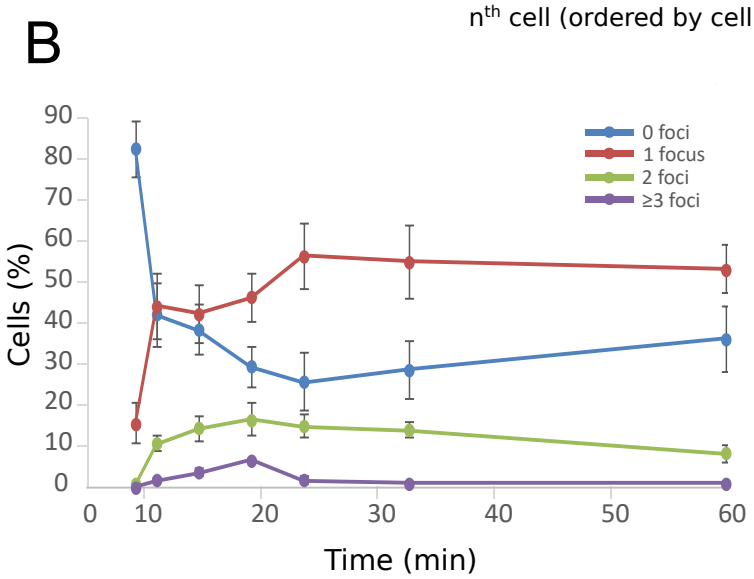

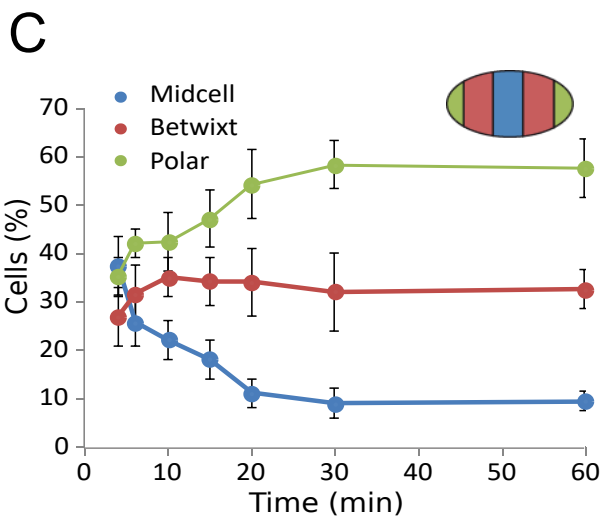

Figure 3

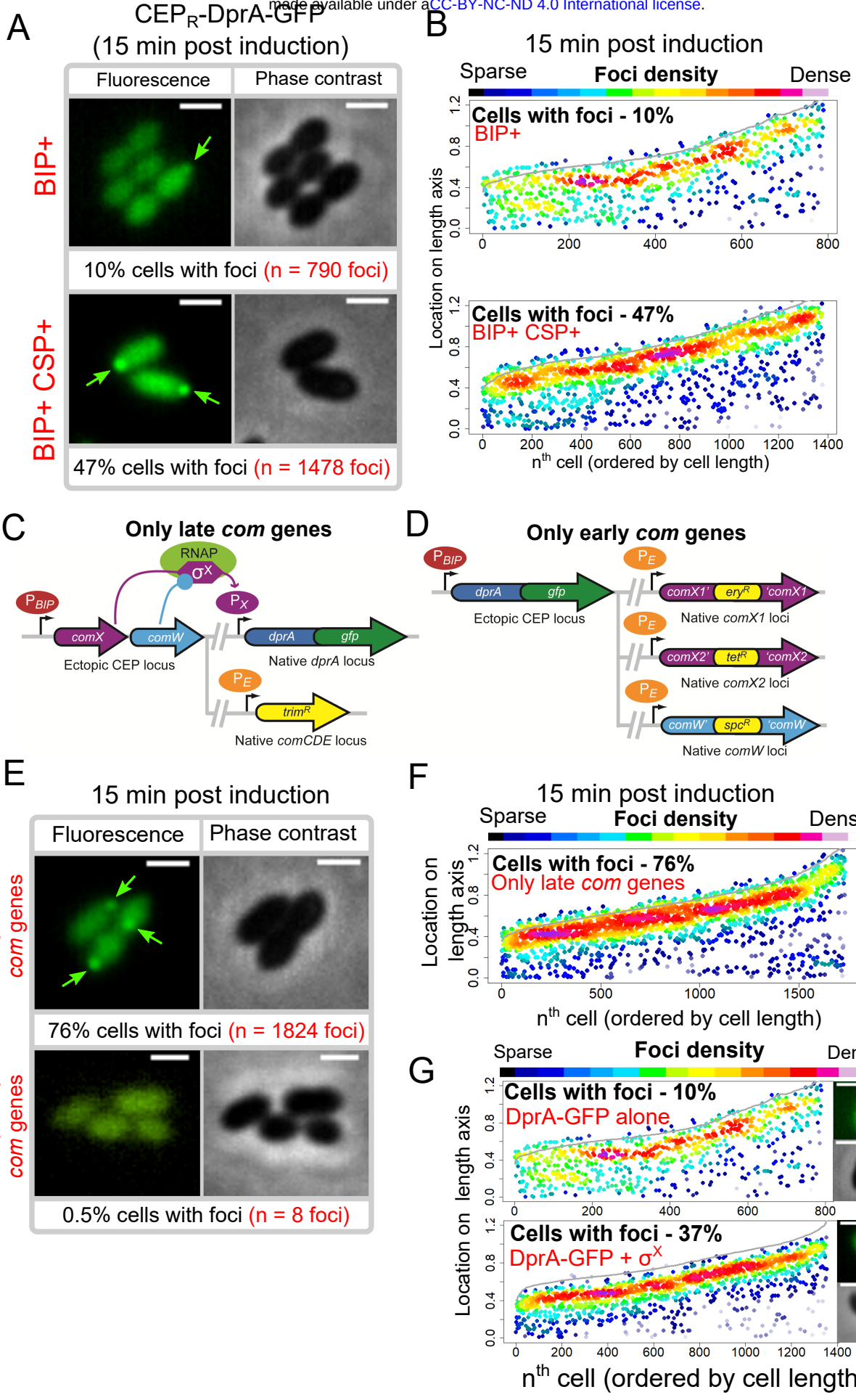

Figure 4

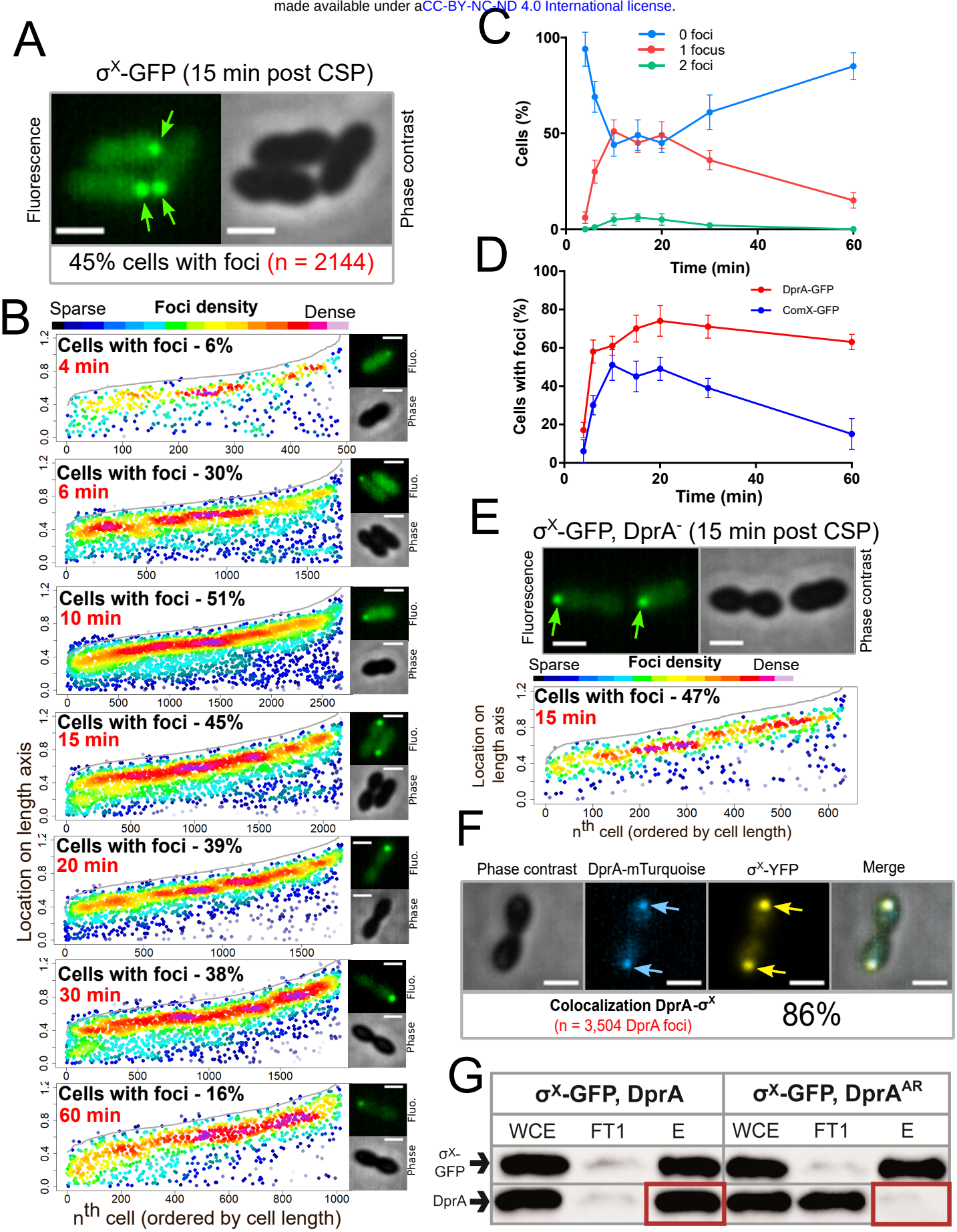

Figure 5

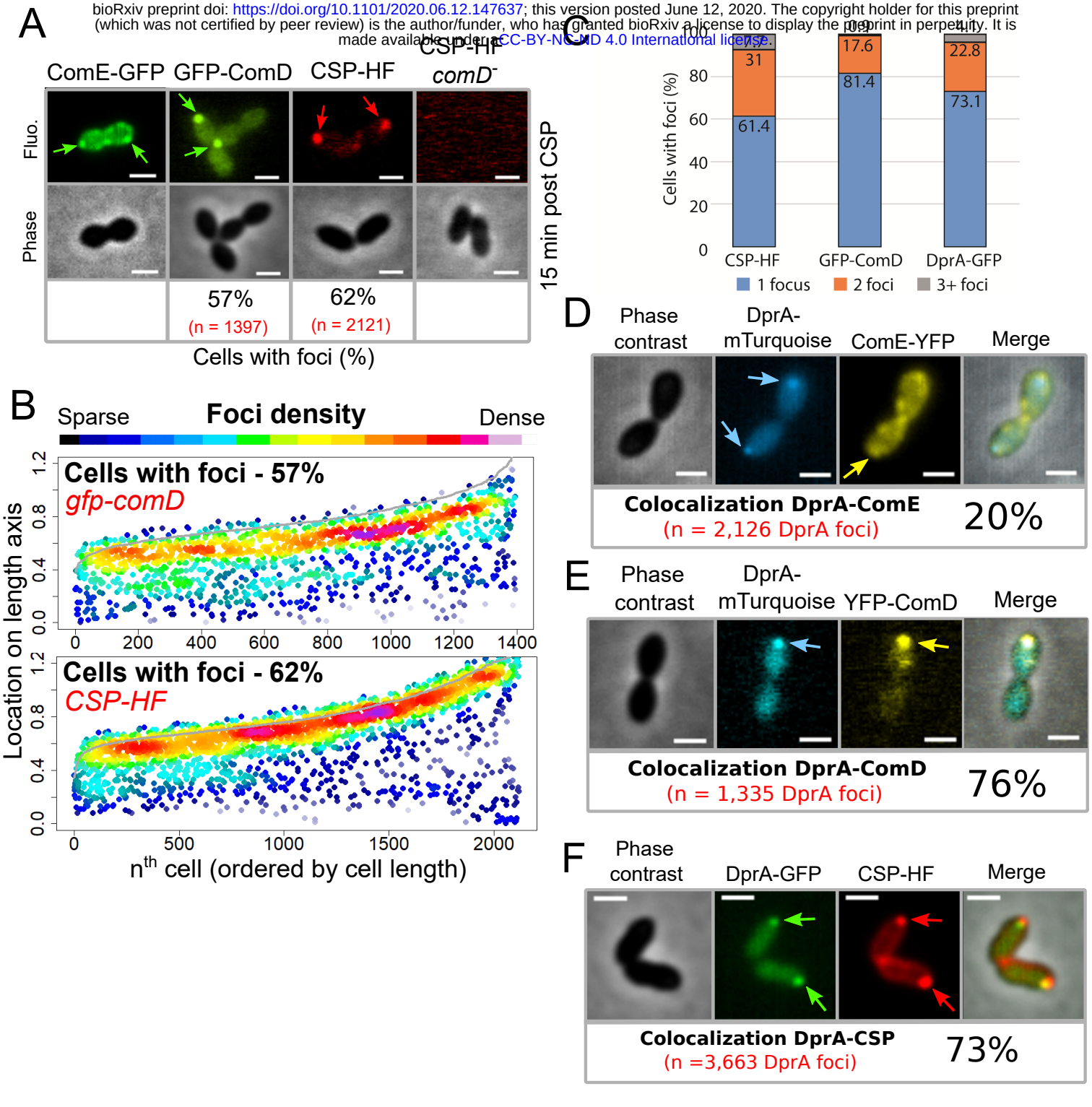

Figure 6

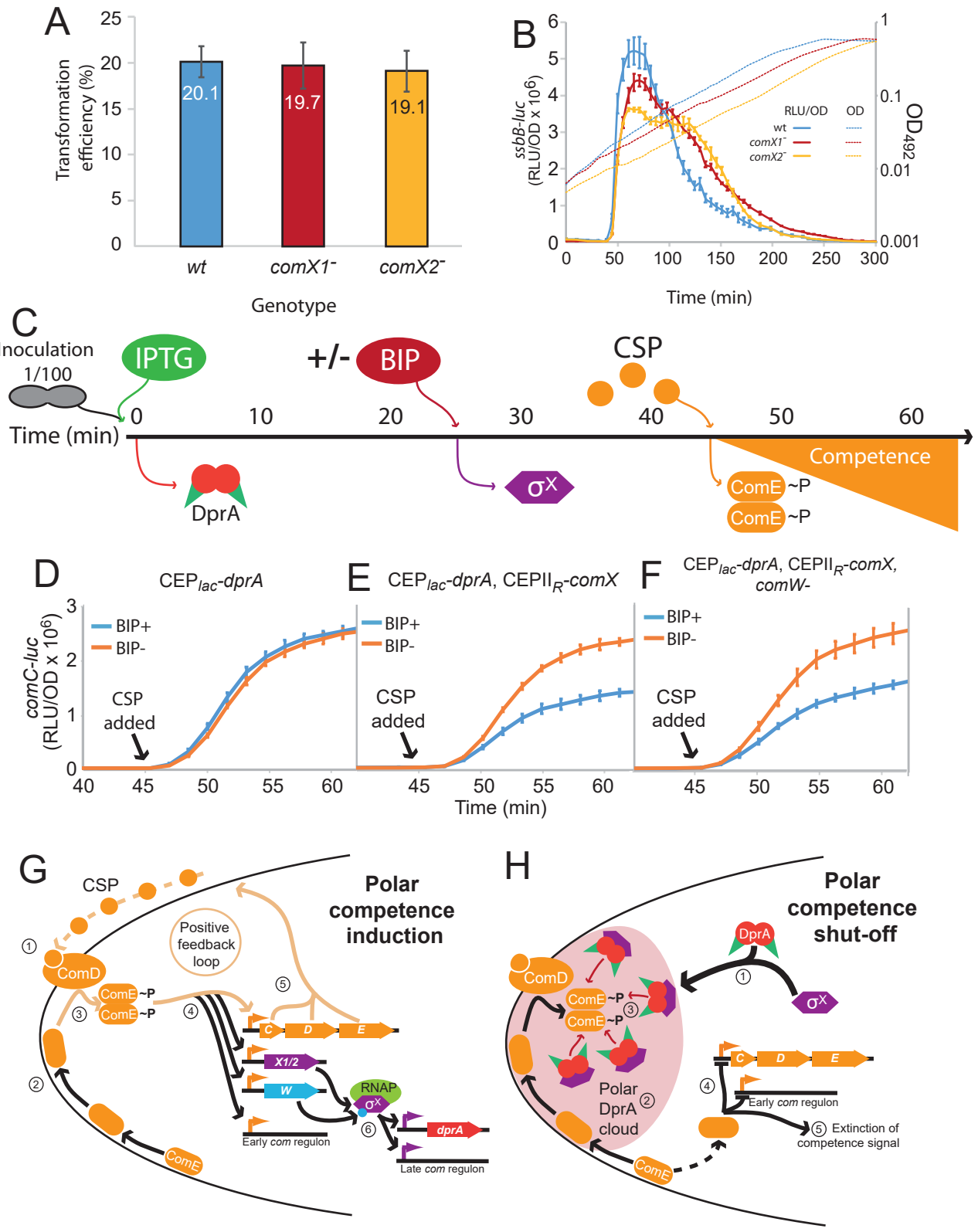

Figure 7

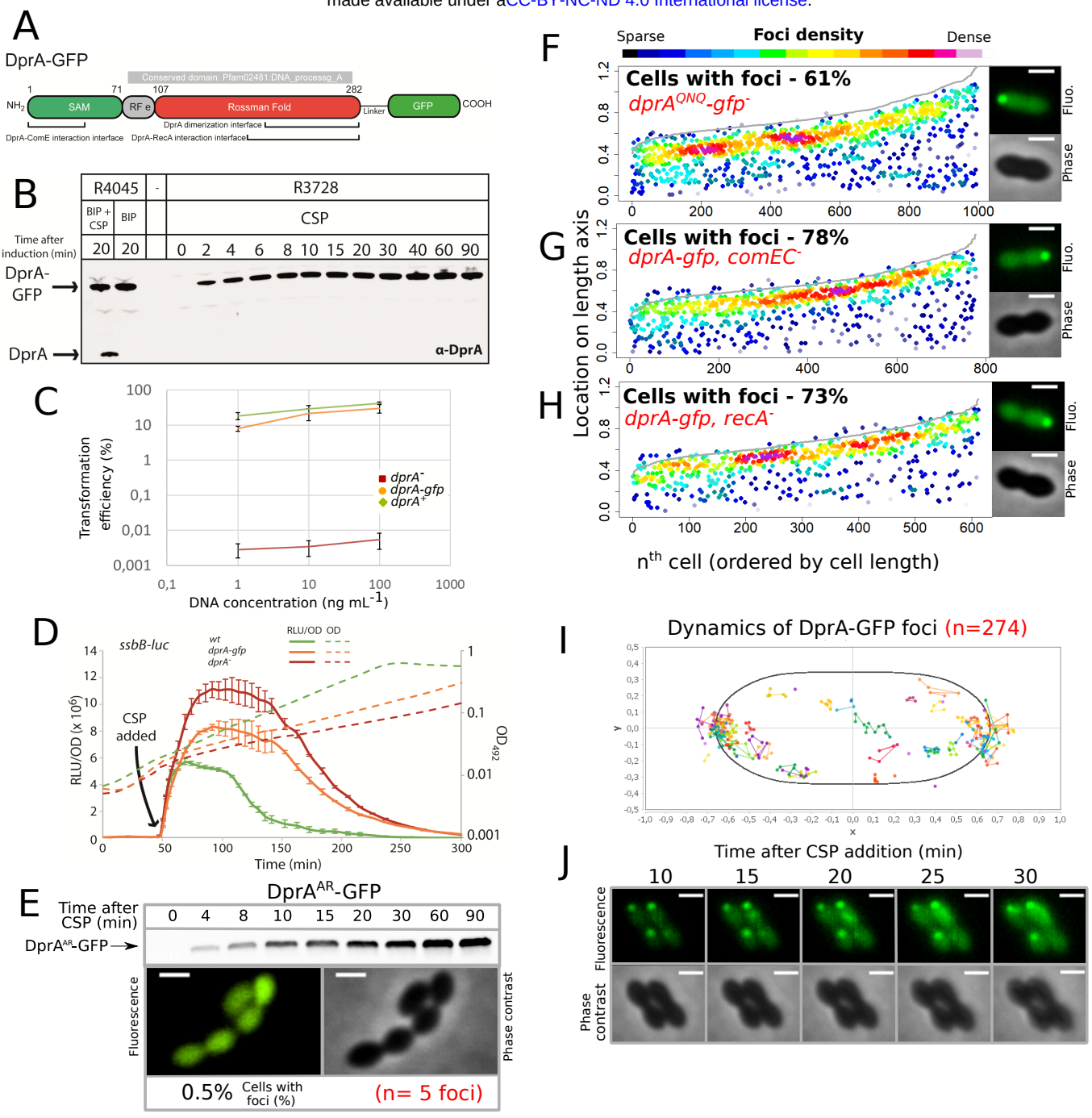

Figure S1

A

B

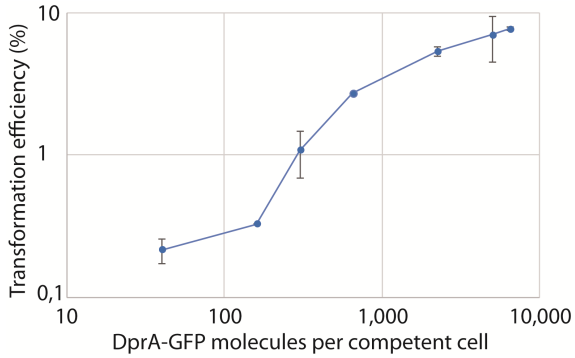

C

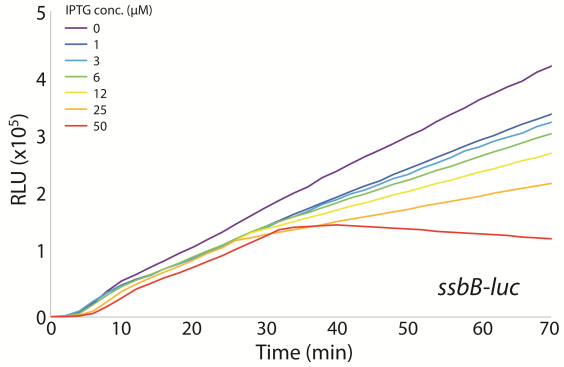

Figure S2

A

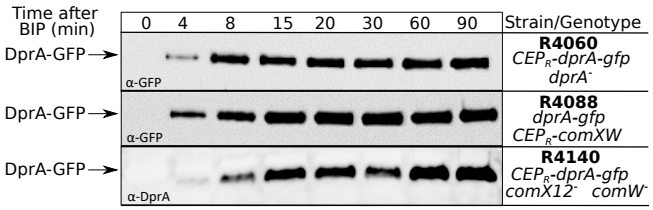

B

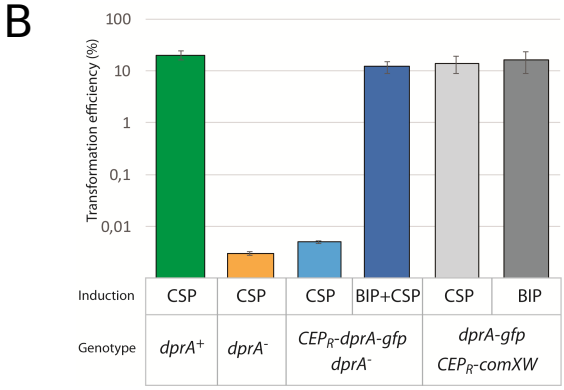

C

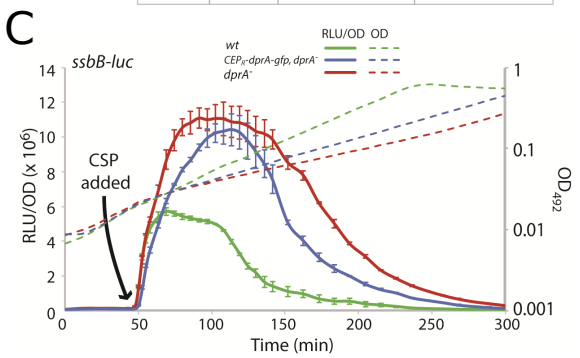

D

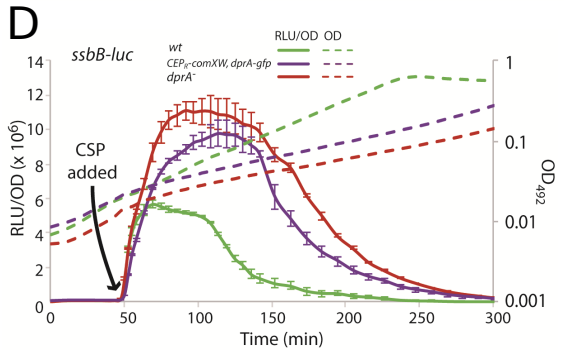

Figure S3

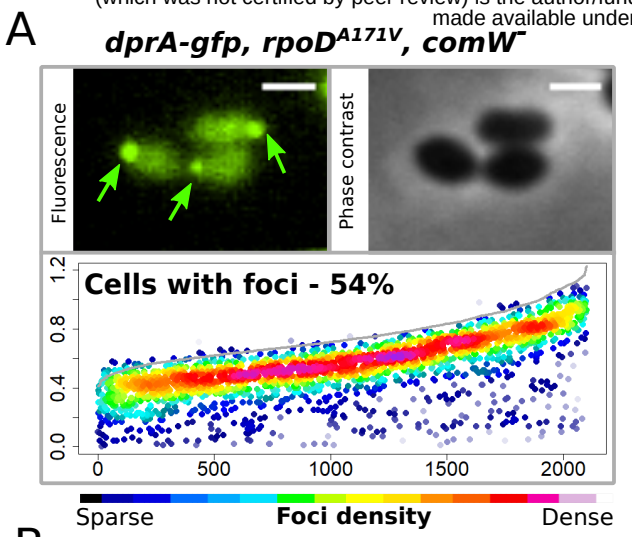

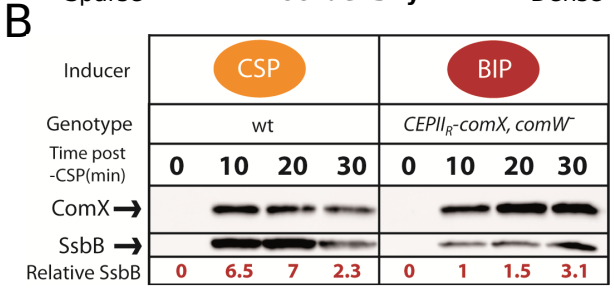

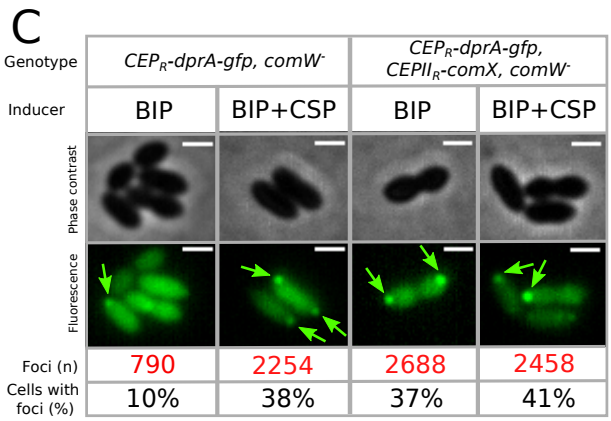

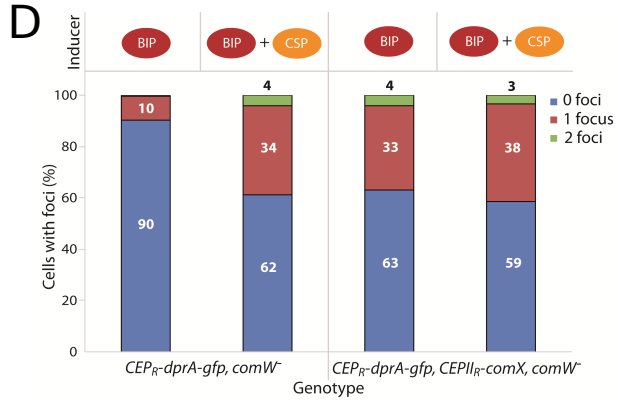

Figure S4

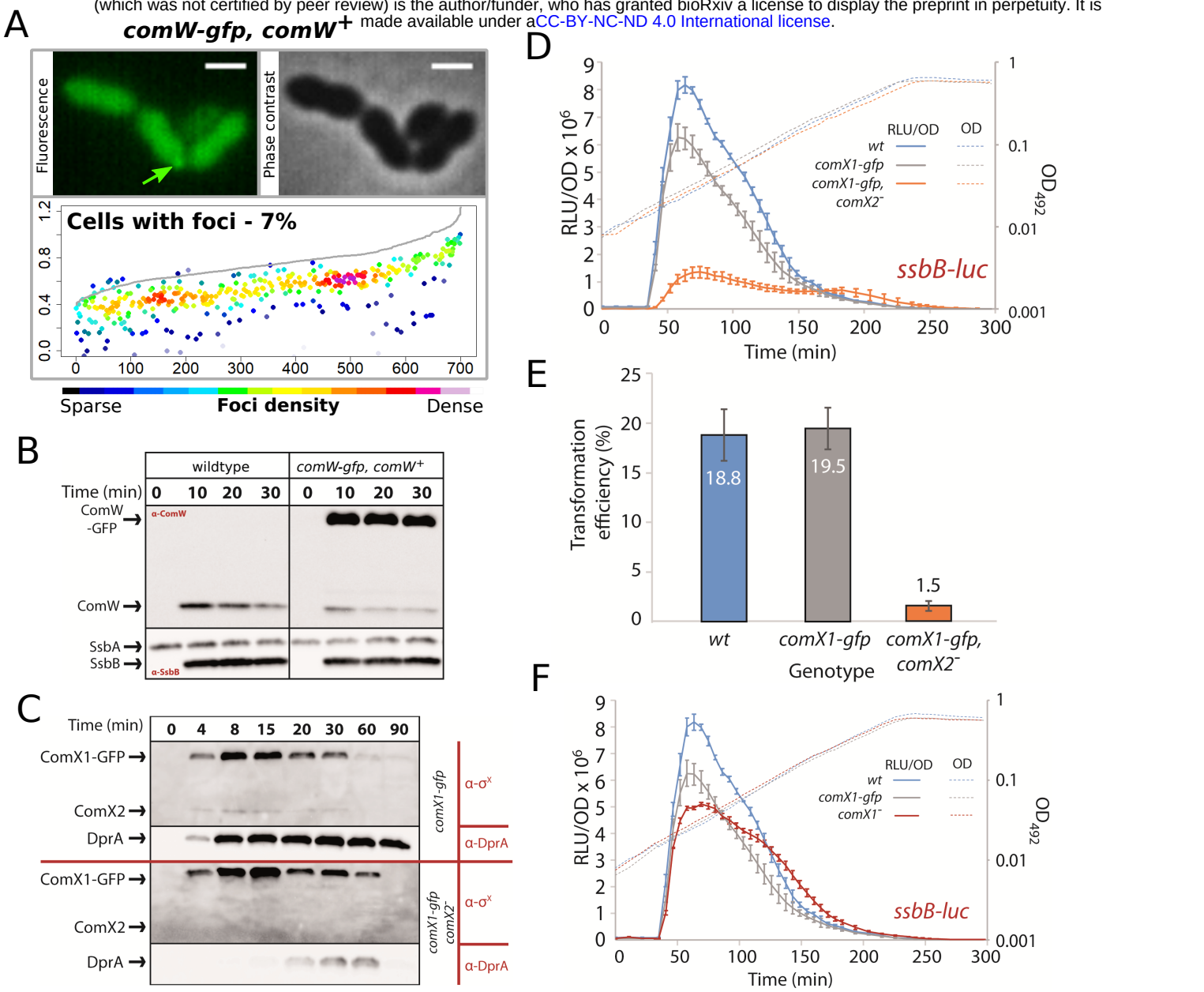

Figure S5

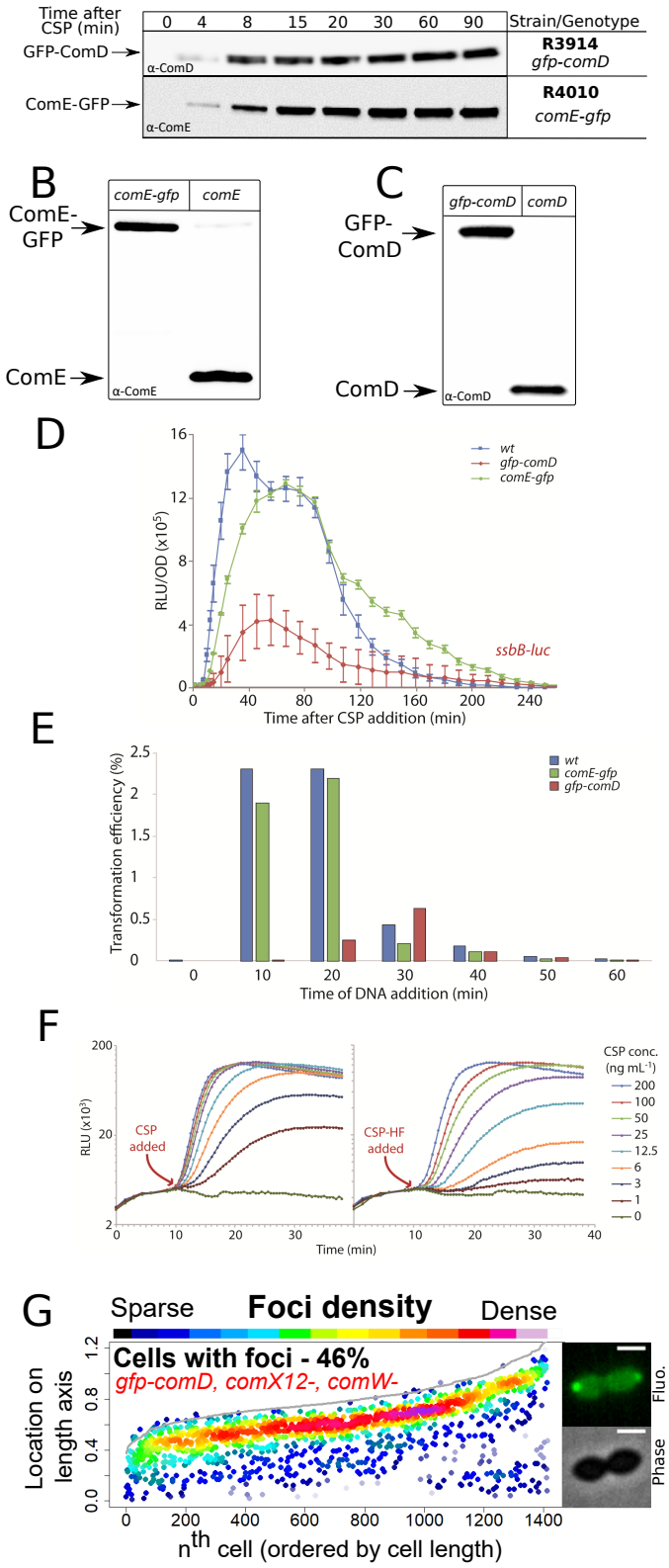

Figure S6

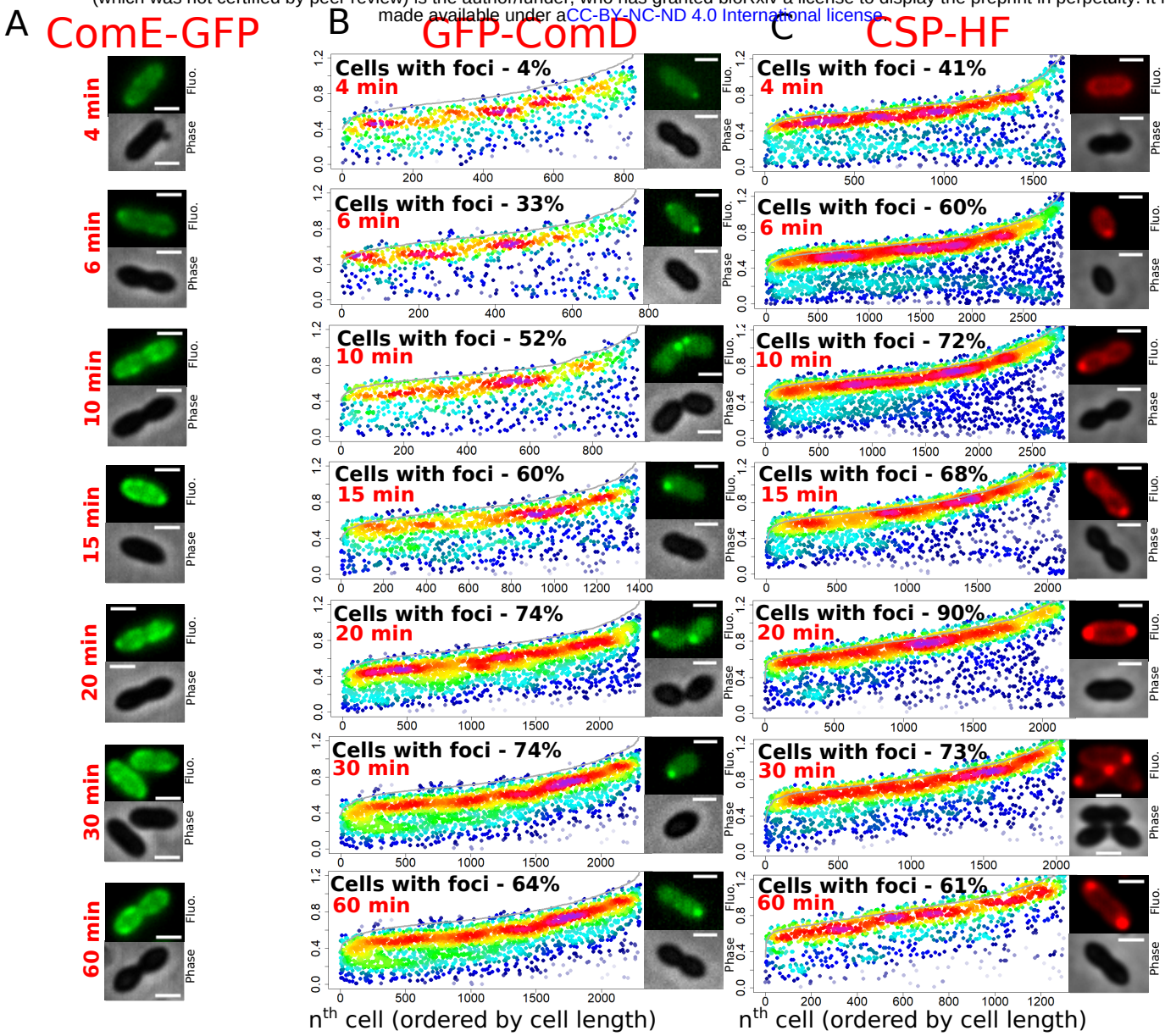

Figure S7

Recipient	Genotype	Protein roles	Transformation efficiency (%)	Expected Transformants	Reference
R4431	*wt*		6,3		
R4434	*comEAC*$^{cinbox-}$	DNA-receptor, transformation pore	0	None	Campbell et al., 1998
R4438	*comGA-GG*$^{cinbox-}$	Transformation pilus	0,00006	Residual	Campbell et al., 1998
R4440	*comFAC*$^{cinbox-}$	DNA-internalizing helicase	0,000022	Residual	Campbell et al., 1998

Table S1: Validation of *cinbox* mutant inactivations.

Strain	Operon	Notable Genes	Protein functions	Reference	Polar DprA foci ?
R4260	*spr0023-0027*	*radA*	Transformation and genome maintenance – Branch migration	(Burghout et al., 2007; Marie et al., 2017)	**Yes**
R4432	*spr0030-0031*				**Yes**
R4433	*spr0126-0128*	*cibABC*	Bacteriocins	(Guiral et al., 2005)	**Yes**
R4441	*spr0182-0183*				**Yes**
R4442	*spr0690*				**Yes**
R4434	*spr0856-0857*	*comEA*	Transformation - DNA capture	(Pestova and Morrison, 1998)	**Yes**
		comEC	Transformation - DNA internalization	(Pestova and Morrison, 1998)	
R4435	*spr0881-0884*	*coiA*	Unknown	(Desai and Morrison, 2006)	**Yes**
R4444	*spr0996*	*radC*	Unknown	(Attaiech et al., 2008)	**Yes**
R4443	*spr1003-spr1111*				**Yes**
R4436	*spr1144*	*dprA*	Transformation, competence shut-off	(Mirouze et al., 2013; Mortier-Barrière et al., 2007)	**Yes**
R4448	*spr1334*				**Yes**
R4445	*spr1628*	*cclA*			**Yes**
R4437	*spr1724*	*ssbB*	Transformation - DNA protection	(Morrison et al., 2007)	**Yes**
R4446	*spr1754-1758*	*cinA*	Unknown		**Yes**
		recA	Recombinase	(Martin et al., 1995)	
		dinF	Unknown		
		lytA	Peptidoglycan hydrolase - autolysis	(Sanchez-Puelles et al., 1986)	
R4447	*spr1831*				**Yes**
R4438	*spr1858-1964*	*comGA-GG*	Transformation pilus proteins	(Laurenceau et al., 2015, 2013)	**Yes**
R4439	*spr2006*	*cbpD*	Peptidoglycan hydrolase, Fratricide	(Guiral et al., 2005)	**Yes**
R4440	*spr2012-2013*	*comFA*	ATP-dependent helicase	(Diallo et al., 2017)	**Yes**
		comFC	Unknown	(Diallo et al., 2017)	

Table S2: Analysis of DprA-mKate2 localization in *cinbox* mutant strains.

Strain	Genotype[a]	Source/Reference	
R209	*recA::cat*; Cm^R	(Martin et al., 1995)	
R304	*rpsL41, rif23, nov1*; Sm^R, Rif^R, Nov^R	(Mortier-Barrière et al., 1998)	
R751	*rpsL1, dprA::spc^{21C}*; Sm^R, Spc^R	(Mirouze et al., 2013)	
R800	Non-capsulated D39 derivative, with 8,651 bp deletion in the *cps* locus	(Lefevre et al., 1979)	
R825	*comC-luc*; Cm^R	(Bergé et al., 2002)	
R895	*ssbB-luc*; Cm^R	(Chastanet et al., 2001)	
R1036	*rpsL1, comC::kan-rpsL*	(Sung et al., 2001)	
R1501	*comC0*	(Dagkessamanskaia et al., 2004)	
R1502	*comC0, ssbB-luc*; Cm^R	(Dagkessamanskaia et al., 2004)	
R1745	*comD::kan^{105}*; Kan^R	(Martin et al., 2013)	
R1818	*comC0, hexA::ermAM*; Ery^R	(Caymaris et al., 2010)	
R2002	*comC0, comC-luc, comX1::ery, comX2::tet*, Cm^R, Tet^R, Ery^R	(Martin et al., 2013)	
R2585	*comC0, dprA^{AR}*	(Quevillon-Cheruel et al., 2012)	
R2830	*comC0, dprA^{QNQ}*	(Quevillon-Cheruel et al., 2012)	
R2018	*comC0, ssbB-luc, dprA::spc^{21C}*; Cm^R, Spc^R	(Martin et al., 2013)	
R3369	*comC2D1*	(Weyder et al., 2018)	
R3728	*comC0, dprA-gfp*; Spc^R	This study	
R3743	*comC0, dprA-gfp, ssbB-luc*; Spc^R, Cm^R	This study	
R3797	*comC2D1, comC-luc, comX1::ery, comW::spc*; Cm^R, Ery^R, Spc^R	This study	
R3833	*comC2D1, CEPlac-dprA, dprA::spc^{21C}*; Kan^R, Spc^R	(Johnston et al., 2018)	
R3912	*comC0, radA-gfp*	This study	
R3914	*rpsl1, gfp-comD*; Sm^R	This study	
R3915	*rpsl1, gfp-comD, ssbB-luc*; Sm^R, Cm^R	This study	
R3932	*comC2D1, CEP$_R$-comXW, ssbB-luc*; Kan^R, Cm^R	(Weyder et al., 2018)	
R4010	*comC0, comE-gfp*	This study	

R4011	*comC0, ssbB-luc, ftsZ-mTurquoise*	(Mortier-Barrière et al., 2019)	
R4015	*comC0, dprA-gfp, hexA::ermAM*; Spc^R, Ery^R	This study	
R4016	*comC0, comE-gfp, hexA::ermAM*; Ery^R	This study	
R4045	*comC0, CEP_R-dprA-gfp*; Kan^R	This study	
R4046	*comC0, dprA-gfp^{AR}*; Spc^R	This study	
R4047	*comC0, dprA-gfp^{QNQ}*; Spc^R	This study	
R4048	*comC0, dprA-mKate2*; Spc^R	This study	
R4060	*comC0, CEP_R-dprA-gfp, dprA::spc^{21C}*; Kan^R, Spc^R	This study	
R4061	*comC0, dprA-gfp, hexA::ermAM, recA::cat*; Spc^R, Ery^R, Cm^R	This study	
R4062	*comC0, dprA-mTurquoise*; Spc^R	This study	
R4076	*comC0, dprA-gfp, hexA::ermAM; CEP_R-comXW*; Spc^R, Ery^R, Kan^R	This study	
R4082	*comC0, dprA-gfp ΔcomEC::kan*; Spc^R, Kan^R	This study	
R4085	*rpsl1, gfp-comD, hexA::ermAM*; Sm^R, Ery^R	This study	
R4087	*comC0, comE-gfp, ssbB-luc*; Cm^R	This study	
R4088	*comC0, dprA-gfp, hexA::ermAM; CEP_R-comXW, cbpD::cat*; Spc^R, Ery^R, Kan^R, Cm^R	This study	
R4091	*comC0, radA$^{cinbox-}$, hexA::ermAM*; Ery^R	This study	
R4095	*rpsl1, gfp-comD, hexA::ermAM, dprA-mTurquoise*; Sm^R, Ery^R, Kan^R	This study	
R4105	*rpsl1, yfp-comD, hexA::ermAM, dprA-mTurquoise*; Sm^R, Ery^R, Spc^R	This study	
R4107	*dprA-gfp, hexA::ermAM; CEP_R-comXW, cbpD::cat,* Δ*comCDE::trim*; Spc^R, Ery^R, Kan^R, Cm^R, $Trim^R$	This study	
R4111	*rpsl1, yfp-comD, hexA::ermAM, dprA-mTurquoise, comA::kan*; Sm^R, Ery^R, Spc^R, Kan^R	This study	
R4112	*rpsl1, gfp-comD, comA::kan*; Sm^R, Kan^R	This study	
R4138	*comC0, CEP_R-dprA-gfp, comX2::tet*; Kan^R, Tet^R	This study	
R4140	*comC0, CEP_R-dprA-gfp, comX2::tet, comX1::ery, comW::spc*; Kan^R, Tet^R, Ery^R, Spc^R	This study	
R4150	*comC0, hexA::ermAM, rpoD^{A171V}*; Ery^R	This study	
R4155	*comC0, hexA::ermAM, rpoD^{A171V}, comW::spc*; Ery^R, Spc^R	This study	
R4166	*comC0, hexA::ermAM, rpoD^{A171V}, comW::cat*; Ery^R, Cm^R	This study	
R4168	*comC0, hexA::ermAM, rpoD^{A171V}, comW::cat, dprA-gfp*; Ery^R, Cm^R, Spc^R	This study	
R4171	*comC0, comE-yfp, hexA::ermAM*; Ery^R	This study	
R4176	*comC0, comE-yfp, hexA::ermAM, dprA-mTurquoise*; Ery^R, Spc^R	This study	
R4222	*comC0, CEP_R-dprA-gfp, dprA::spc^{21C}, ssbB-luc*; Kan^R, Spc^R, Cm^R	This study	

R4260	*comC0, dprA-gfp, hexA::ermAM, radC^{cin-}*; Spc^R, Ery^R	This study	
R4261	*comC0, CEP$_{lac}$-dprA-gfp;* Kan^R	This study	
R4262	*comC0, CEP$_{lac}$-dprA-gfp, dprA::spc^{21C}*; Kan^R, Spc^R	This study	
R4265	*comC0, radA$^{cinbox-}$, hexA::ermAM, dprA-gfp*; Ery^R, Spc^R	This study	
R4402	*comC2D1, CEPlac-dprA-gfp, dprA::spc^{21C}, ssbB-luc*; Kan^R, Spc^R, Cm^R	This study	
R4431	*comC0, radA-gfp, dprA-mKate2*; Spc^R	This study	
R4432	*comC0, radA-gfp, dprA-mKate2, spr0031$^{cinbox-}$*; Spc^R	This study	
R4433	*comC0, radA-gfp, dprA-mKate2, cibA$^{cinbox-}$*; Spc^R	This study	
R4434	*comC0, radA-gfp, dprA-mKate2, comEA$^{cinbox-}$*; Spc^R	This study	
R4435	*comC0, radA-gfp, dprA-mKate2, coiA$^{cinbox-}$*; Spc^R	This study	
R4436	*comC0, radA-gfp, dprA-mKate2, radA$^{cinbox-}$*; Spc^R	This study	
R4437	*comC0, radA-gfp, dprA-mKate2, ssbB$^{cinbox-}$*; Spc^R	This study	
R4438	*comC0, radA-gfp, dprA-mKate2, comGA$^{cinbox-}$*; Spc^R	This study	
R4439	*comC0, radA-gfp, dprA-mKate2, cbpD$^{cinbox-}$*; Spc^R	This study	
R4440	*comC0, radA-gfp, dprA-mKate2, comFA$^{cinbox-}$*; Spc^R	This study	
R4441	*comC0, radA-gfp, dprA-mKate2, spr0182$^{cinbox-}$*; Spc^R	This study	
R4442	*comC0, radA-gfp, dprA-mKate2, spr0690$^{cinbox-}$*; Spc^R	This study	
R4443	*comC0, radA-gfp, dprA-mKate2, spr1003$^{cinbox-}$*; Spc^R	This study	
R4444	*comC0, radA-gfp, dprA-mKate2, radC$^{cinbox-}$*; Spc^R	This study	
R4445	*comC0, radA-gfp, dprA-mKate2, cclA$^{cinbox-}$*; Spc^R	This study	
R4446	*comC0, radA-gfp, dprA-mKate2, cinA$^{cinbox-}$*; Spc^R	This study	
R4447	*comC0, radA-gfp, dprA-mKate2, spr1831$^{cinbox-}$*; Spc^R	This study	
R4448	*comC0, radA-gfp, dprA-mKate2, spr1334 $^{cinbox-}$*; Spc^R	This study	
R4451	*comC0, comX1-gfp*	This study	
R4461	*comC0, comX1-gfp, comX2::tet*; Tet^R	This study	
R4465	*comC0, comX1-gfp, comX2::tet, ssbB-luc*; Tet^R, Cm^R	This study	
R4466	*comC0, ssbB-luc, comX1::ery*; CmR, Ery^R	This study	
R4467	*comC0, ssbB-luc, comX2::tet*; CmR, Tet^R	This study	
R4468	*comC0, comX1-gfp, hexA::ermAM*; Ery^R	This study	
R4469	*comC0, comX1-gfp, ΔdprA::kan*; Kan^R	This study	
R4471	*comC0, comX1-gfp, ssbB-luc*; Cm^R	This study	
R4472	*comC0, comX1-yfp, hexA::ermAM*; Ery^R	This study	

R4473	*comC0, comX1-yfp, hexA::ermAM, dprA-mTurquoise*; Ery^R, Spc^R	This study	
R4489	*comC0, CEP_R-dprA-gfp, dprA::spc^{21C}, $CEPII_R$-comX*; Kan^R, Spc^R, Ery^R	This study	
R4492	*comC0, CEP_R-dprA-gfp, dprA::spc^{21C}, comC-luc*; Kan^R, Spc^R, Cm^R	This study	
R4493	*comC0, CEP_R-dprA-gfp, dprA::spc^{21C}, $CEPII_R$-comX, comC-luc*; Kan^R, Spc^R, Ery^R, Cm^R	This study	
R4498	*comC2D1, CEP_{lac}-dprA, dprA::spc^{21C}, $CEPII_R$-comX*; Kan^R, Spc^R, Ery^R	This study	
R4500	*comC2D1, CEP_{lac}-dprA, dprA::spc^{21C}, $CEPII_R$-comX, comC-luc*; Kan^R, Spc^R, Ery^R, Cm^R	This study	
R4509	*comC2D1, CEP_{lac}-dprA, dprA::spc^{21C}, $CEPII_R$-comX, comC-luc, ΔcomW::trim*; Kan^R, Spc^R, Ery^R, Cm^R, $Trim^R$	This study	
R4511	*comC2D1, CEP_{lac}-dprA, dprA::spc^{21C}, comC-luc*; Kan^R, Spc^R, Cm^R	This study	
R4513	*comC0, comW-gfp, comW$^+$*	This study	
R4514	*comC0, comX1-gfp, hexA::ermAM, dprA^{AR}*; Ery^R	This study	
R4573	*comC0, dprA-gfp, hexA::ermAM; CEP_R-comXW, ssbB-luc*; Spc^R, Ery^R, Kan^R, Cm^R	This study	
R4574	*ΔcomCDE::trim*; $Trim^R$	This study	
R4575	*comC0, ΔcomW::trim*; $Trim^R$	This study	
Plasmid	**Genotype**	**Source/reference**	
pAO0	pUC19 derivative with *spc* gene under control of strong pneumococcal promoter; Spc^R	This study	
pEMcat	Plasmid carrying Cm^R in a minitransposon cassette for *mariner* mutagenesis; Cm^R	(Akerley et al., 1998)	
pMB42	pAO0-derived plasmid possessing *'dprA-gfp*; Spc^R	This study	
pMB42-dprA^{AR}	pMB42 possessing *dprA^{AR}* sequence	This study	
pMB42-dprA^{QNQ}	pMB42 possessing *dprA^{QNQ}* sequence	This study	
pMB42-mTurquoise	pMB42 possessing *mTurquoise* sequence	This study	
pMB42-mKate2	pMB42 possessing *mKate2* sequence	This study	
pCEP$_R$-luc	pCEP derivative with the *luc* gene under control of P_R; Kan^R, Spc^R	(Johnston et al., 2016)	
pCEP$_R$-dprA-gfp	pCEP$_R$-luc derivative with *luc* replaced by *dprA-gfp*; Kan^R, Spc^R	This study	
pCEP$_R$-comXW	pCEP$_R$-luc derivative with *luc* replaced by *comX* and *comW*; Kan^R, Spc^R	This study	
pCEPlac-dprA-gfp	pCEPR-dprA-gfp derivative with P_R replaced with P_{lac}, as well as a P_{syn} promoter controlling *lacI* expression; KanR, Spc^R	This study	

pUC57-CEPII$_R$-comX	pUC57 derivative with P$_R$-*comX* and Ery^R flanked by sequences homologous to *cpsN* and *cpsO*; Amp^R, Ery^R	Genscript, USA	
pMK111	*bgaA'-P$_{Zn}$-tet^R-mKate2-parBp^{mut}-m(sf)gfp, 'bgaA*; Amp^R, Kan^R	(van Raaphorst et al., 2017)	
Primer	**Sequence (5'-3')[b]**	**Source/reference**	***Use***
BM105	ATTCGCAAGCTTTCCCTTGAACTAGTCGAAG	(Guiral et al., 2006)	*CEP$_{lac}$-dprA-gfp*
CJ379	AGTTTTGGAAGTATTTTGTCATCTA	This study	*comE-gfp*
CJ380	CCTTTAGAAACCATTCCGGAACCCTCGAGCTTTTGAGATTTTTTCTCTAAAATATCTT	This study	*comE-gfp*
CJ381	AAGATATTTTAGAGAAAAAATCTCAAAAGCTCGAGGGTTCCGGAATGGTTTCTAAAGG	This study	*comE-gfp*
CJ382	CATTATATCAATTTCTTGCTAATTGTCAATTATTTATACAATTCATCCATACCATGTG	This study	*comE-gfp*
CJ383	CACATGGTATGGATGAATTGTATAAATAATTGACAATTAGCAAGAAATTGATATAATG	This study	*comE-gfp*
CJ384	CTATCAAAGAAGTAGAAGTAATAGG	This study	*comE-gfp*
CJ385	TTACAAGAAAAAACATTTTAGGAGA	This study	Δ*comCDE::trim*
CJ410	GCG*CCATGG*CCTAATTAGCTGAAGGAGGAATA	This study	*CEP$_R$-dprA-gfp*
CJ411	GCG*GGATCC*TTATTTATACAATTCATCCATACCAT	This study	*CEP$_R$-dprA-gfp*
CJ431	GCG*CTCGAG*TCTAGAGGATCTGGTGGAGAAGCTGCAGC	This study	*dprA-mkate2*
CJ432	GCG*AAGCTT*TTAACGGTGTCCCAATTTACTAGGCAAAT	This study	*dprA-mkate2*
CJ454	GCG*CTCGAG*TTATTTATACAATTCATCCATACC	This study	*dprA-mTurquouise*
CJ455	GCG*CTCGAG*ATGGTTTCTAAAGGTGAAGAATTG	This study	*dprA-mTurquouise*
CJ471	TCTAGAACTAGTGGATCCCCCGGGCTGCAGATAATAAAATCTCCTAAAATGTTTTTTCTT	This study	Δ*comCDE::trim*
CJ472	AAGAAAAAACATTTTAGGAGATTTTATTATCTGCAGCCCGGGGGATCCACTAGTTCTAGA	This study	Δ*comCDE::trim*
CJ473	TCACTTTTGAGATTTTTTCTCTAAAATATCTCAAAGCTTATCGATACCGTCGACCTCGAG	This study	Δ*comCDE::trim*
CJ474	CTCGAGGTCGACGGTATCGATAAGCTTTGAGATATTTTAGAGAAAAAATCTCAAAAGTGA	This study	Δ*comCDE::trim*
CJ496	ACCTTTAGAAACCATTCCGGAACCCTCGAGAAATTCAAATTCCGCAAGAACATCTTGCC	This study	*CEP$_{lac}$-dprA-gfp*
CJ497	GGCAAGATGTTCTTGCGGAATTTGAATTTCTCGAGGGTTCCGGAATGGTTTCTAAAGGT	This study	*CEP$_{lac}$-dprA-gfp*
CJ498	ACATTATCCATTAAAAATCAAACGGATCCTTATTTATACAATTCATCCATACCATGTG	This study	*CEP$_{lac}$-dprA-gfp*
CJ499	CACATGGTATGGATGAATTGTATAAATAAGGATCCGTTTGATTTTTAATGGATAATGT	This study	*CEP$_{lac}$-dprA-gfp*
CJ500	GCGCCAAGAGGAAGGATTGATCAA	This study	*CEP$_{lac}$-dprA-gfp*
CJ508	GTCGCTCATTAAAAGGTCAGTTAAT	This study	*comW-gfp*
CJ513	CTAAAATATTTGTTTGTTCACGACC	This study	*comW-gfp*
CJ514	CCTTTAGAAACCATTCCGGAACCCTCGAGACAAGAAATAAACCCCCGATTCATTACCA	This study	*comW-gfp*

CJ515	TGGTAATGAATCGGGGGTTTATTTCTTGT*CTCGAG*GGTTCCGGAATGGTTTCTAAAGG	This study	*comW-gfp*
CJ516	AATTAGTTCGGAAATTTACTAAAATTACCTTATTTATACAATTCATCCATACCATGTG	This study	*comW-gfp*
CJ517	CACATGGTATGGATGAATTGTATAAATAAGGTAATTTTAGTAAATTTCCGAACTAATT	This study	*comW-gfp*
CJ559	GCGGATGAAACAGGATTCGATACTTAT	This study	Δ*comW::trim*
CJ560	TCTAGAACTAGTGGATCCCCCGGGCTGCAGAATCAAATACTCCTTTTCTTTTTTATAAA	This study	Δ*comW::trim*
CJ561	TTTATAAAAAAGAAAAGGAGTATTTGATTCTGCAGCCCGGGGGATCCACTAGTTCTAGA	This study	Δ*comW::trim*
CJ562	AATTAGTTCGGAAATTTACTAAAATTACCAAGCTTATCGATACCGTCGACCTCGAGGG	This study	Δ*comW::trim*
CJ563	CCCTCGAGGTCGACGGTATCGATAAGCTTGGTAATTTTAGTAAATTTCCGAACTAATT	This study	Δ*comW::trim*
CJ564	GCGCCGTCTATAGTATACCCGACCTAT	This study	Δ*comW::trim*
CJ643	GCGATACATGATTGCACTTCCTAAAGA	This study	*comX1-gfp*
CJ644	TCTTCACCTTTAGAAACCATTCCGGAACC*CTCGAG*ATGGGTACGGATAGTAAACT	This study	*comX1-gfp*
CJ645	AGTTTACTATCCGTACCCAT*CTCGAG*GGTTCCGGAATGGTTTCTAAAGGTGAAGA	This study	*comX1-gfp*
CJ646	ATTTTTTTCATTTTTTTTGCATGACTTATTATTTATACAATTCATCCATACCATGT	This study	*comX1-gfp*
CJ647	ACATGGTATGGATGAATTGTATAAATAATAAGTCATGCAAAAAAAATGAAAAAAAT	This study	*comX1-gfp*
CJ648	GCGGAGAGCCGCTTTCGCCACCGGTGT	This study	*comX1-gfp*
DDL48	GTGATATAATAAAAAGAGAAGAAATATGACTGTACGTCAT	This study	*spr0031*$^{cinbox-}$
DDL49	CAAGTATTTTTCAAACTTTTA*GGATCC*TAATAGATAGAGCCAGAGAAT	This study	*spr0031*$^{cinbox-}$
DDL50	ATTCTCTGGCTCTATCTATTA*GGATCC*TAAAAGTTTGAAAAATACTTG	This study	*spr0031*$^{cinbox-}$
DDL51	ATTTTCGCTGAGTTTTTCAAGTAAAATAGGCTCTGTTTCT	This study	*spr0031*$^{cinbox-}$
DDL52	CCGATGGCAAAAACGCCGACTTCTTCAGGTTTAAGAGTGT	This study	*cibA*$^{cinbox-}$
DDL53	GCTCACTTTTCCTTTTCTTTA*GGATCC*TTAAAAGTGAACAAGAAAAAA	This study	*cibA*$^{cinbox-}$
DDL54	TTTTTTCTTGTTCACTTTTAA*GGATCC*TAAAGAAAAGGAAAAGTGAGC	This study	*cibA*$^{cinbox-}$
DDL55	TCACGTCCTCTTCGGTAATCCCTGCTTCTGCCAATGCCTC	This study	*cibA*$^{cinbox-}$
DDL56	CTCACACTTGCTTCAATGTTGAATGAATTAGACATAAGAG	This study	*comEA*$^{cinbox-}$
DDL57	TATTTTCTCCTCTCTTAGATA*GGATCC*TAGAGGAAGAAAAAACAGTCG	This study	*comEA*$^{cinbox-}$
DDL58	CGACTGTTTTTTCTTCCTCTA*GGATCC*TATCTAAGAGAGGAGAAAATA	This study	*comEA*$^{cinbox-}$
DDL59	AGTCAGCCATTTCAACTTTTCTTGGGTCAAGCCCAATCGC	This study	*comEA*$^{cinbox-}$
DDL60	GATAAGCGTAAGCATTCACAAAAAGACAAGAAGAAAAAAG	This study	*coiA*$^{cinbox-}$
DDL61	AATTCCCTCCTTTTCTATATA*GGATCC*TAAAAAGAAAAAAGATCAGGA	This study	*coiA*$^{cinbox-}$
DDL62	TCCTGATCTTTTTTCTTTTTA*GGATCC*TATATAGAAAAGGAGGGAATT	This study	*coiA*$^{cinbox-}$
DDL63	GCTCCAGCCAATAATTCTTCTTCACGTTGTGAAAGAACGT	This study	*coiA*$^{cinbox-}$
DDL64	TTTGTCAAGGTCTTTGAATTCTTTCTTAAACAAGCCTTGT	This study	*dprA*$^{cinbox-}$

DDL65	TTTGATTTTTTACGAACTTTA*GGATCC*TGATAGATGAGTAGAAAAAGA	This study	*dprA*$^{cinbox-}$
DDL66	TCTTTTTCTACTCATCTATCA*GGATCC*TAAAGTTCGTAAAAAATCAAA	This study	*dprA*$^{cinbox-}$
DDL67	CTCTTGGTAAAAGAAGGGAAAGTTCGCCTCTCAATTTTCTTAAATATT	This study	*dprA*$^{cinbox-}$
DDL68	CTGTGAAAGGTAACCACGGTCAAACTGCATTCCTTCTACG	This study	*ssbB*$^{cinbox-}$
DDL69	TGTAACTTTTTTTGATTTCCA*GGATCC*TGATAAGTAGGAGGAAGAAAA	This study	*ssbB*$^{cinbox-}$
DDL70	TTTTCTTCCTCCTACTTATCA*GGATCC*TGGAAATCAAAAAAAGTTACA	This study	*ssbB*$^{cinbox-}$
DDL71	ACAATGATTTTTACGTATAACAAAGAACATGTCGGTGATG	This study	*ssbB*$^{cinbox-}$
DDL72	GAAAAGACACTCATCTTAGAACTTCTTTTATAAAAAGTGA	This study	*comGA*$^{cinbox-}$
DDL73	TTTTTATTTTTCTAACTCTTA*GGATCC*TGTATAGGTGAGGAGGTAAGT	This study	*comGA*$^{cinbox-}$
DDL74	ACTTACCTCCTCACCTATACA*GGATCC*TAAGAGTTAGAAAAATAAAAA	This study	*comGA*$^{cinbox-}$
DDL75	ACTTGCCAAAGTGGTACCATTCTTGGCCACGAAGGGATTG	This study	*comGA*$^{cinbox-}$
DDL76	TGATAGCGCAAAATAAGAAAAATGTCAAGGAAACTGCTTA	This study	*cbpD*$^{cinbox-}$
DDL77	TTCTCACTTTTTCTTTTTTCAA*GGATCC*TTTTAGGTGAAGGCAATCATC	This study	*cbpD*$^{cinbox-}$
DDL78	GATGATTGCCTTCACCTAAAA*GGATCC*TTGAAAAAAGAAAAAGTGAGAA	This study	*cbpD*$^{cinbox-}$
DDL79	GTGGTGATGCCATAGATGCAACAACGGTTCGTACTATCCT	This study	*cbpD*$^{cinbox-}$
DDL80	CACTTTGTTGACAACTCTGTTTTCATACAATTTGGACAGT	This study	*comFA*$^{cinbox-}$
DDL81	TCATCTAAAGTGCTAGTTTTA*GGATCC*TTAGAAGTATGAAAGTAAATTT	This study	*comFA*$^{cinbox-}$
DDL82	AAATTTACTTTCATACTTCTAA*GGATCC*TAAAACTAGCACTTTAGATGA	This study	*comFA*$^{cinbox-}$
DDL83	CTAATCCATCTTTACCGAAAGCAGCTAGTATCTCAGCTCC	This study	*comFA*$^{cinbox-}$
DDL84	ATGGCTCCCATTTTATGGATTACTGTCCTCATTCTACTGA	This study	*spr0182*$^{cinbox-}$
DDL85	ATTCCCCTCCTCTTTCTTTCA*GGATCC*TAAAGACAAGAAAAATAGGTC	This study	*spr0182*$^{cinbox-}$
DDL86	GACCTATTTTTCTTGTCTTTA*GGATCC*TGAAAGAAAGAGGAGGGGAAT	This study	*spr0182*$^{cinbox-}$
DDL87	CCGTATTTGTCTCCTCTTTTACCAAATCAGCAAGACGATT	This study	*spr0182*$^{cinbox-}$
DDL88	GATATTTTAACCCTCTTTCCAGAGATGTTTTCTCCACTGG	This study	*spr0690*$^{cinbox-}$
DDL89	CTTTTTTAGTTTCATTAGTTA*GGATCC*TAAATCTTGTAGATTTTAGGA	This study	*spr0690*$^{cinbox-}$
DDL90	TCCTAAAATCTACAAGATTTA*GGATCC*TAACTAATGAAACTAAAAAAG	This study	*spr0690*$^{cinbox-}$
DDL91	ACAGAAGAGCAAGCTATTAAAGAATACGGTCAAGACCAAA	This study	*spr0690*$^{cinbox-}$
DDL92	AGTCGATAATGGCGATAGGAGCATCAAGATATTCAGCCAG	This study	*spr1003*$^{cinbox-}$
DDL93	ATTTTGCTTACGATATTGCTA*GGATCC*TCCACGAAGTTTAATCTTTAA	This study	*spr1003*$^{cinbox-}$
DDL94	TTAAAGATTAAACTTCGTGGA*GGATCC*TAGCAATATCGTAAGCAAAAT	This study	*spr1003*$^{cinbox-}$
DDL95	GGCCAGCAATCCCTTAGAAACCTCGTGCTTTTTTAAAAAG	This study	*spr1003*$^{cinbox-}$
DDL96	GAAAATTACCGCTCAACCAAAACCATTCTTCAAGCGGCCA	This study	*radC*$^{cinbox-}$

DDL97	AAAAATCCTCCTCACTTTATA*GGATCC*TAGAAGGATGGAAAATTAGAT	This study	*radC*$^{cinbox-}$
DDL98	ATCTAATTTTCCATCCTTCTA*GGATCC*TATAAAGTGAGGAGGATTTTT	This study	*radC*$^{cinbox-}$
DDL99	TCGTTCAGTATGTCGATTTGACAAGTGAACTCCAAACCCT	This study	*radC*$^{cinbox-}$
DDL101	ACAGCATGAAGCAGACTCAGTAAGCCTTCAAGATCGCGTA	This study	*cclA*$^{cinbox-}$
DDL102	AAAAATCAATCATACTTATCA*GGATCC*TAAAAATGGGAGAAATAGTAT	This study	*cclA*$^{cinbox-}$
DDL103	ATACTATTTCTCCCATTTTTA*GGATCC*TGATAAGTATGATTGATTTTT	This study	*cclA*$^{cinbox-}$
DDL104	TGAGGAATTGGCTCTTTATGCCAGGGAAAAATTAGGTATT	This study	*cclA*$^{cinbox-}$
DDL105	TTGCTCCGCACGTTCACCCAAACGCATGATTGATCCTTTA	This study	*cinA*$^{cinbox-}$
DDL106	CTGCGATTTTTTCAAAAAAAA*GGATCC*TGATAGGTAGGAGGAAACATG	This study	*cinA*$^{cinbox-}$
DDL107	CATGTTTCCTCCTACCTATCA*GGATCC*TTTTTTTTGAAAAAATCGCAG	This study	*cinA*$^{cinbox-}$
DDL108	AGGAGATGGAAATATTCCTCAACAAGCAAGCTAGTTCGGA	This study	*cinA*$^{cinbox-}$
DDL109	GCATCCCAGAGCTTCCCATCAATCTCGCCACTATCATCTT	This study	*rmuC*$^{cinbox-}$
DDL110	TTAAAAAAGTGTACGCTTCTT*GGATCC*TTATAGATAGGGAAGTGTCGG	This study	*rmuC*$^{cinbox-}$
DDL111	CCGACACTTCCCTATCTATAA*GGATCC*AAGAAGCGTACACTTTTTTAA	This study	*rmuC*$^{cinbox-}$
DDL112	ACACCAGGATTTTCATCCTTGGACTATGAAGTATCAAGGG	This study	*rmuC*$^{cinbox-}$
DDL114	GGAGCTCAAGCCGTCAATTGGGGAGCTTCAGGAGGGGCTA	This study	*spr1831*$^{cinbox-}$
DDL115	TTTATTTTTTTATTTTTCATA*GGATCC*TATATAGATGAAGGGGAAAGA	This study	*spr1831*$^{cinbox-}$
DDL116	TCTTTCCCCTTCATCTATATA*GGATCC*TATGAAAAATAAAAAAATAAA	This study	*spr1831*$^{cinbox-}$
DDL117	ATCGAAAAAATCTTCTGGATGCGTTTTGAACCAGTAGTCC	This study	*spr1831*$^{cinbox-}$
DDL118	TTTTCGAGTAAGTACGAAGATTGGATAACATCAAAGAAAG	This study	*spr1334*$^{cinbox-}$
DDL119	ATAAGCTATTAGCTTTCTTTA*GGATCC*TAATAGATAGAAGCATAGAAT	This study	*spr1334*$^{cinbox-}$
DDL120	ATTCTATGCTTCTATCTATTA*GGATCC*TAAAGAAAGCTAATAGCTTAT	This study	*spr1334*$^{cinbox-}$
DDL121	GTTTAATGAGTTCAAAGATACGGCCAGGAGTTCCAATCAG	This study	*spr1334*$^{cinbox-}$
dprA22	CT*GAATTC*TAGATGACTGTTATCCTTG	This study	pMB42
dprA23	TCA*CTCGAG*AAATTCAAATTCCGCAAGAACATC	This study	pMB42
MB117	AATCTCCGCTGTAGGTCACTTTCTT	(Marie et al., 2017)	*rpsL41*
MB120	TTGGATTGGGTGTGCATTTGC	(Marie et al., 2017)	*rpsL41*
MP216	ATGAAAATTAAAGTTGTAACAGTTGGG	This study	*gfp-comD*
MP217	CAATTCTTCACCTTTAGAAACCATTACTCTTTCCCCTTATTTCATTACT	This study	*gfp-comD*
MP218	GTAATGAAATAAGGGGAAAGAGTAATGGTTTCTAAAGGTGAAGAATTG	This study	*gfp-comD*
MP219	TCCGGAACC*CTCGAG*TTTATACAATTCATCCATACCATG	This study	*gfp-comD*
MP220	CATGGTATGGATGAATTGTATAAA*CTCGAG*GGTTCCGGAATGGATTTATTTGGATTTGGGACGG	This study	*gfp-comD*

MP221	GCATAGACAATTGACTGAGCAACC	This study	*gfp-comD*
OMB4	AGA*CTCGAG*GGTTCCGGAATGGTTTCTAAAGGTGAAG	(Mirouze et al., 2013)	pMB42
OMB5	TGT*AAGCTT*GGATTATTTATACAATTCATCCATACCATGTG	This study	pMB42

Table S3: Strains, plasmids and primers used in this study.

[a] Antibiotic resistances: Spc^R, spectinomycin; Kan^R, kanamycin; $Trim^R$, trimethoprim; Sm^R, streptomycin; Cm^R, chloramphenicol; Rif^R, rifampicin; Nov^R, novobiocin; Ery^R, erythromycin; Tet^R, tetracycline; Amp^R, ampicillin.

[b] Underlined, italic bases represent restriction sites used for cloning.